Organic & Biomolecular Chemistry

ROYAL SOCIETY OF CHEMISTRY

PAPER

View Article Online
View Journal

Cite this: DOI: 10.1039/d0ob01557a

Discovery of new pyrimidine-5-carbonitrile derivatives as anticancer agents targeting EGFR^{WT} and EGFR^{T790M}†

Ahmed A. Nasser,[a] Ibrahim H. Eissa, *[a] Mohamed R. Oun,[a] Mohamed A. El-Zahabi,*[a] Mohammed S. Taghour,[a] Amany Belal,[b] Abdulrahman M. Saleh,[a] Ahmed B. M. Mehany,[c] Hendrik Luesch,[d,e] Ahmad E. Mostafa,[f] Wael M. Afifi,[f,g] James R. Rocca[d,h] and Hazem A. Mahdy*[a]

A new series of pyrimidine-5-carbonitrile derivatives has been designed as ATP mimicking tyrosine kinase inhibitors of the epidermal growth factor receptor (EGFR). These compounds were synthesized and evaluated for their *in vitro* cytotoxic activities against a panel of four human tumor cell lines, namely colorectal carcinoma (HCT-116), hepatocellular carcinoma (HepG-2), breast cancer (MCF-7), and non-small cell lung cancer cells (A549). Five of the synthesized compounds, **11$_a$**, **11$_b$**, **12$_b$**, **15$_b$** and **16$_a$**, were found to exhibit moderate antiproliferative activity against the tested cell lines and were more active than the EGFR inhibitor erlotinib. In particular, compound **11$_b$** showed 4.5- to 8.4-fold erlotinib activity against HCT-116, HepG-2, MCF-7, and A549 cells with IC_{50} values of 3.37, 3.04, 4.14, and 2.4 μM respectively. Moreover, the most cytotoxic compounds that showed promising IC_{50} values against the four cancer cell lines were subjected to further investigation for their kinase inhibitory activities against EGFR^{WT} and EGFR^{T790M} using homogeneous time resolved fluorescence (HTRF) assay. Compound **11$_b$** was also found to be the most active compound against both EGFR^{WT} and mutant EGFR^{T790M}, exhibiting IC_{50} values of 0.09 and 4.03 μM, respectively. The cell cycle and apoptosis analyses revealed that compound **11$_b$** can arrest the cell cycle at the G2/M phase and induce significant apoptotic effects in HCT-116, HepG-2, and MCF-7 cells. Additionally, compound **11$_b$** upregulated the level of caspase-3 by 6.5 fold in HepG-2 when compared with the control. Finally, molecular docking studies were carried out to examine the binding mode of the synthesized compounds against the proposed targets; EGFR^{WT} and EGFR^{T790M}. Additional *in silico* ADMET studies were performed to explore drug-likeness properties.

Received 29th July 2020,
Accepted 11th September 2020

DOI: 10.1039/d0ob01557a

rsc.li/obc

1. Introduction

Cancer treatment is considered as one of the greatest medical challenges, although there have been great advances in this field. The cancer problem progressively affects low- and middle-income countries, and poor persons within all nations, reflecting the original socio-economic relationship.[1] It is the second major cause of death worldwide, exceeded only by heart diseases.[2] According to the WHO, cancer is the second leading cause of death all over the world, accounting for 9.6 million deaths in 2018. The number of affected persons over the next twenty years is expected to increase by around 70%.[3]

Cancer arises when normal cells lose their regulatory mechanisms which control their proliferation.[4] Protein kinases (PKs) play a vital role in the regulation of cellular functions such as cell proliferation, metabolism, survival, and apoptosis.[5] Such enzymes facilitate the transfer of the

[a]*Pharmaceutical Medicinal Chemistry & Drug Design Department, Faculty of Pharmacy (Boys), Al-Azhar University, Cairo 11884, Egypt. E-mail: Ibrahimeissa@azhar.edu.eg, malzahaby@yahoo.com, Hazem_hady2001@azhar.edu.eg*
[b]*Medicinal Chemistry Department, Faculty of Pharmacy, Beni-Suef University, Beni-Suef 62514, Egypt*
[c]*Zoology Department, Faculty of Science, Al-Azhar University, Cairo 11884, Egypt*
[d]*Department of Medicinal Chemistry, University of Florida, Gainesville, FL 32610, USA*
[e]*Center for Natural Products, Drug Discovery and Development (CNPD3), University of Florida, Gainesville, FL 32610, USA*
[f]*Pharmacognosy and Medicinal Plants Dept., Faculty of Pharmacy (Boys), Al-Azhar University, Cairo, 11884, Egypt*
[g]*Department of Pharmacognosy, Faculty of Pharmacy, Sinai University, Ismailia, Egypt*
[h]*AMRIS Facility, McKnight Brain Institute, University of Florida, Gainesville, FL 32610, USA*

†Electronic supplementary information (ESI) available. See DOI: 10.1039/d0ob01557a

γ-phosphate group from ATP to particular threonine, serine, or tyrosine hydroxyl groups on target protein substrates involved in a number of cell signaling pathways.[6] Disrupting cell signaling cascades through kinase alterations (especially hyper-activation, hyper-production, or mutation) leads to many diseases, including cancer.[7]

One of the most important protein kinases is the epidermal growth factor receptor (EGFR), which plays a crucial role in cell proliferation and migration.[8,9] The EGFR is overexpressed in many human solid tumors such as breast cancer,[5] non-small cell lung cancer (NSCLC)[10] and hepatocellular carcinoma (HCC).[11] Modern molecular strategies have been designed to target specific molecules affecting regulatory mechanisms involved in the control of cancer cell proliferation. These strategies enable the improvement of cancer therapy efficiency compared to conventional chemotherapy and/or radiotherapy protocols. The aim of targeted therapies is inhibition and downregulation of overactive proteins responsible for triggering of aberrant cellular pathways,[12–14] and hence, EGFRs are considered as promising targets for the design of new antitumor agents.[15–19]

Upon examination of the clinically used EGFR-tyrosine kinase inhibitors (EGFR-TKIs) (Fig. 1), it was found that, most of these inhibitors have some problems. For example, the first-generation EGFR-TKI, erlotinib **1**[20] and gefitinib **2**[21] showed ocular side effects, trichomegaly,[22] and life-threatening side-effect interstitial lung disease (ILD).[23] In addition, the anticancer efficacy of such drugs was reduced due to the acquired drug resistance caused by EGFR-TK mutation.[24] This mutation decreases the binding of an ATP-competitive inhibitor to the kinase and restores ATP affinity to the EGFR.[25] In order to overcome drug resistance induced by $EGFR^{T790M}$, the second-generation had been developed including neratinib **3**[26] and pelitinib **4**.[27] Most of these inhibitors comprise electrophilic Michael-acceptor moieties that could form a covalent bond with Cys797 at the lip of the ATP binding cleft of EGFR causing the inactivation of the protein.[28–30] However, they showed a relatively low maximal-tolerated-dose (MTD) due to the non-selective inhibition against wild-type EGFR-TK ($EGFR^{WT}$) and the mutant type $EGFR^{T790M}$, leading to poor clinical patient outcomes.[31,32]

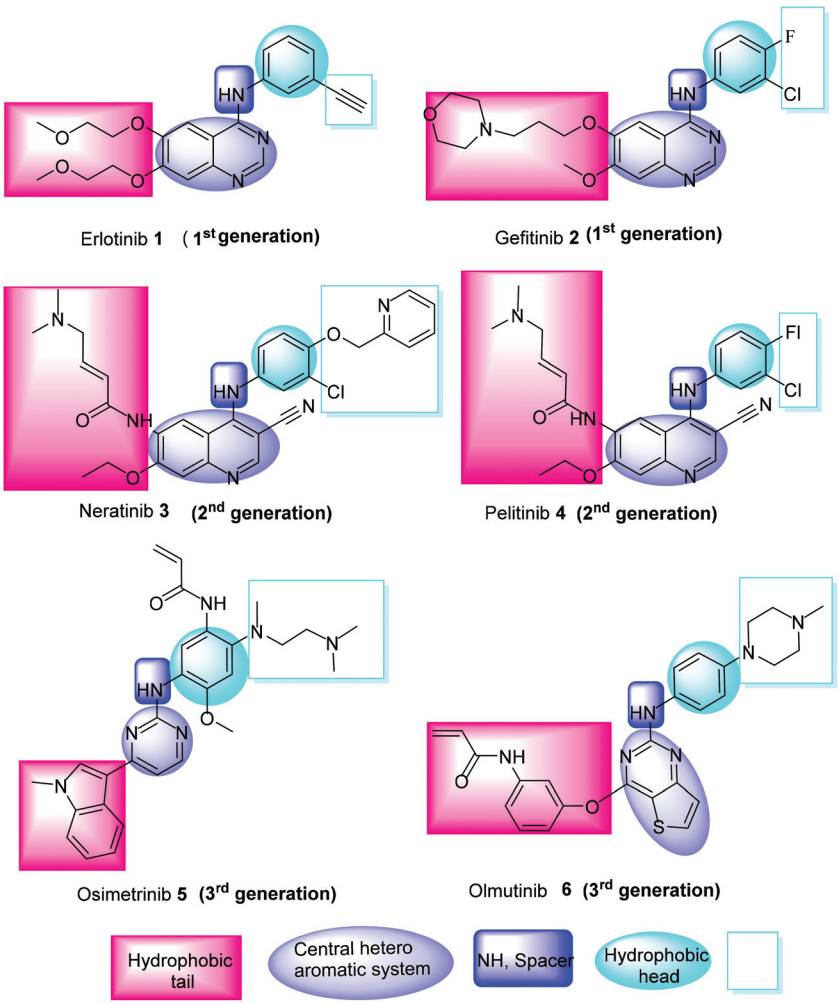

Fig. 1 Some reported EGFR-TK inhibitors and their basic pharmacophoric features.

Moreover, the third-generation irreversible EGFR-TKIs, osimertinib **5**[33] and olmutinib **6** have shown improved activities towards $EGFR^{T790M}$ over $EGFR^{WT}$. Unfortunately, in 2016, a safety alert about olmutinib was recorded, in which two cases of toxic epidermal necrolysis (one of which was fatal) and a case of Stevens–Johnson syndrome were described.[34] Accordingly, there is a great demand to modify the existing EGFR-TKIs to obtain more potent and less toxic candidates.

Pyrimidines are important building blocks in many pharmaceuticals for the synthesis of antineoplastic agents,[35–38] including EGFR-TKIs.[39–43] Similarly, the related substituted pyrimidine nucleus is an important pharmacophore, presented in a number of anticancer agents.[44] Moreover, a literature survey revealed that the thiopyrimidine-5-carbonitrile ring system has occupied a marked position in the design and synthesis of novel chemotherapeutic agents with remarkable antitumor effects.[36,45,46] In addition, 4-anilinothiopyrimidine-5-carbonitrile and 4-hydrazinothiopyrimidine-5-carbonitrile and their condensed heterocycles exerted promising anticancer activity.[38,47]

The nitrile group (CN) is an important pharmacophore, present in a number of anticancer agents, including the EGFR inhibitors neratinib **3**[26] and pelitinib **4**,[27] aromatase inhibitors fadrozole monohydrochloride and letrozole for the treatment of breast cancer,[48] and a nonsteroidal androgen receptor antagonist bicalutamide for the treatment of advanced prostate cancer.[49] Some reports state that nitrile-based inhibitors are good candidates for the development of reversible covalent inhibitors with SH and OH containing biomolecules such as proteases,[50,51] cysteine,[52,53] and serine amino acids[54] (ESI†). Hence, in our design, the CN group was inserted to act as an electrophilic center toward a free nucleophilic amino acid. This is necessary to form a covalent bond with the conserved cysteine residue present in the lip of the EGFR ATP binding site (Cys797).

Based on our previous research in the field of design and synthesis of new anticancer agents,[12–14,55–63] and attractiveness of tyrosine kinases as promising targets for the design of new anti-cancer agents, we decided to introduce new pyrimidine-5-carbonitrile derivatives that may exhibit good inhibitory activities against wild-type EGFR-TK ($EGFR^{WT}$) and mutant EGFR-TK ($EGFRT^{790M}$).

1.1. Rationale of molecular design

The ATP binding pocket of EGFR-TK consists of five main regions – (a) an adenine binding pocket contains key amino acids which can form hydrogen bonds with the adenine ring, (b) a sugar region (hydrophilic ribose pocket), (c) hydrophobic region I, though not used by ATP but plays an important role in inhibitor selectivity, (d) hydrophobic region II, not used by ATP and may be exploited for inhibitor specificity, and (e) a phosphate binding region – which can be used for improving inhibitor pharmacokinetics (Fig. 2).[64–66] A study of the structure–activity relationships (SAR) and common pharmacophoric features shared by various EGFR-TKIs revealed that, most EGFR-TKIs are Y-shaped[67] and share four common pharmacophoric features as shown in Fig. 1 and 3.[68]

In addition, the common pharmacophoric features of EGFR-TKIs are: (i) a flat hetero-aromatic system, occupying the adenine binding pocket. This hetero-aromatic system can participate in hydrogen bonding interactions with Met793, Thr854, and Thr790 residues.[69] (ii) A terminal hydrophobic head to be inserted in the hydrophobic region I.[68] (iii) An imino group (NH, spacer) which can form important hydrogen bond interactions with amino acid residues in the linker

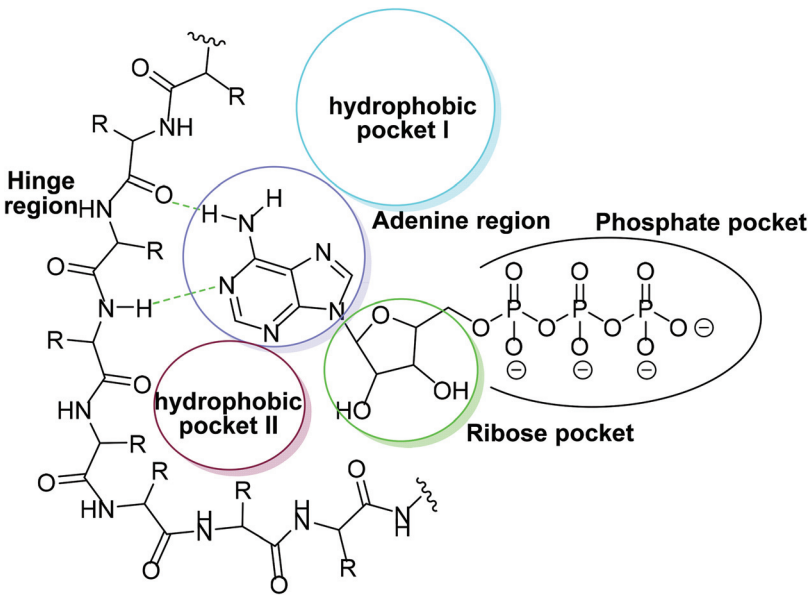

Fig. 2 ATP binding site of a EGFR-TK cavity composed of five main features.[65]

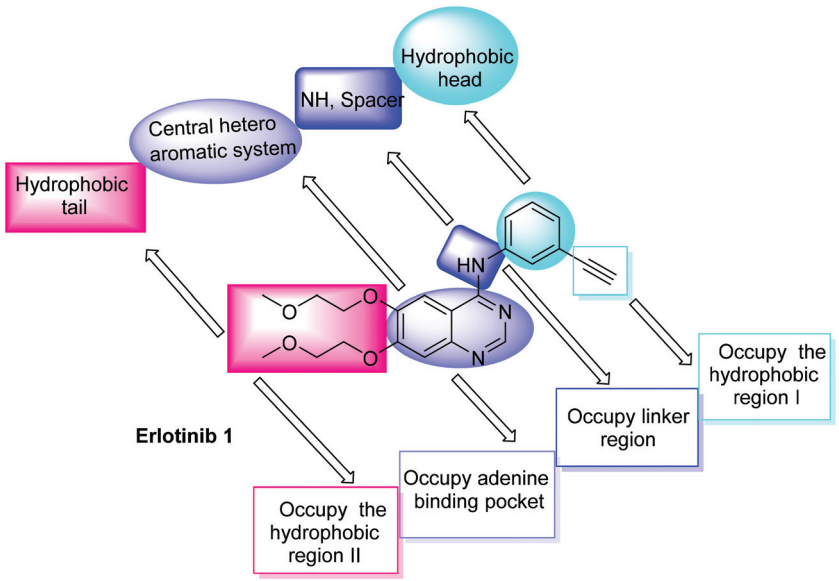

Fig. 3 The basic structural requirements for erlotinib as a reported EGFR-TK inhibitor.[12]

region.[70] (iv) A hydrophobic tail which occupies the hydrophobic region II.[64,71]

In this work, a series of pyrimidine-5-carbonitrile derivatives having the essential pharmacophoric features of EGFR-TKIs have been designed and synthesized. Such derivatives comprised structural modifications of erlotinib **1** at four different positions (Fig. 4).

The first position was the quinazoline moiety (hetero-aromatic system), where this nucleus was replaced by a pyrimidine ring as a biological isostere to occupy the adenine binding region.[67,72] The second position was the terminal phenyl ring (hydrophobic head), where different substituted phenyl, aromatic heterocyclic, or aliphatic structures were used. The third position was the NH linker, where different hydrogen bond donors were utilized. The used linkers may be one atom (imino group as in compounds **10**$_{a–h}$, **11**$_{a,b}$, **12**$_{a,b}$, **13**$_{a,b}$, **14**$_{a,b}$, **15**$_{a,b}$, and **16**$_{a,b}$), two atoms (hydrazinyl group as in compounds **18**$_{a,b}$ and the methyl amino group as in compounds **17**$_{a,b}$), or three atoms (ethyl amino group as in compounds **19**$_{a,b}$). The fourth position was the two 2-methoxyethoxy groups (hydrophobic tail), where a phenyl ring was incorporated at position-6 of the pyrimidine nucleus to occupy the hydrophobic region II of the ATP binding site. It is worth mentioning that the bulkiness of the pyrimidine nucleus was modified by alkyl substitution on SH groups at position-2 with ethyl and butyl groups.

All modifications encouraged us to study the structure–activity relationship of the synthesized compounds as anticancer agents. The overall design and modification are illustrated in Fig. 4 and 5. The most active compounds were examined for their anti-proliferative activities against a number of human cancer cell lines. Promising compounds were examined for their activities against EGFR^{WT} and EGFR^{T790M} and the most active compound was tested for its ability to induce apoptosis. Furthermore, a molecular docking was performed to rationalize and emphasize the mechanism of action of the synthesized compounds as EGFR-TKIs.

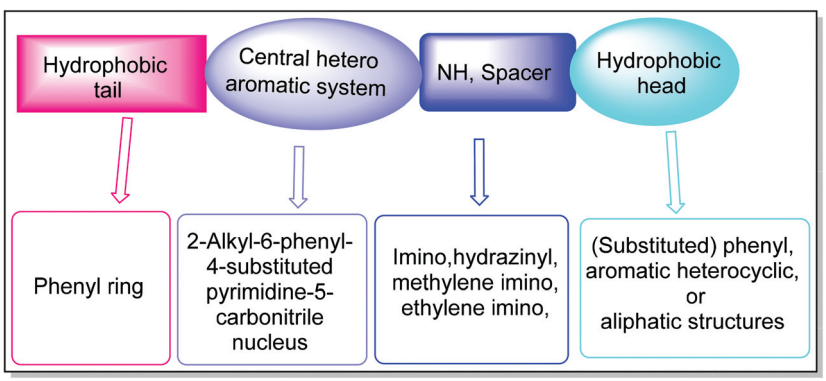

Fig. 4 Summary of the possible modifications of EGFR-TK inhibitors.

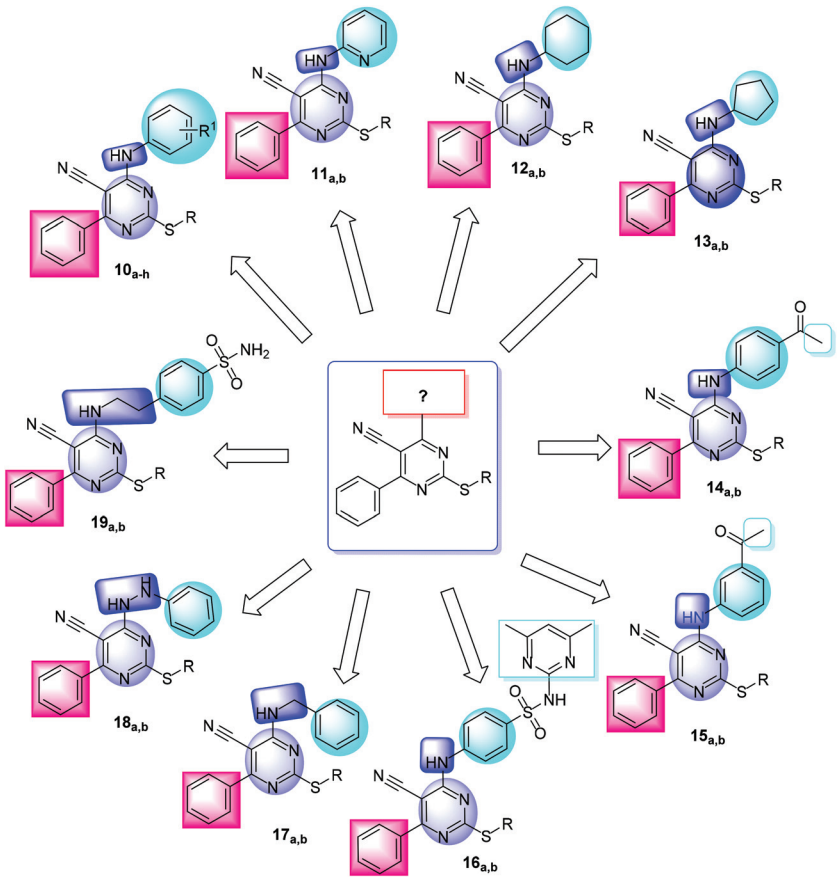

Fig. 5 Rationale of the molecular design of the new proposed EGFR-TK inhibitors.

2. Results and discussion

2.1. Chemistry

The synthetic routes adopted for the synthesis of the designed compounds are outlined in Schemes 1, 2 and 3. For the preparation of compounds 7, $\mathbf{8_{a,b}}$ and $\mathbf{9_{a,b}}$ (Scheme 1), the key starting compound (4-oxo-6-phenyl-2-thioxo-1,2,3,4-tetrahydro-pyrimidine-5-carbonitrile) 7 was synthesized by one-pot reaction of thiourea, ethylcyanoacetate and benzaldehyde in refluxing ethanol containing potassium carbonate according to a reported method.[73,74] Selective *S*-alkylation of compound 7 using bromoethane or bromobutane in 10% alc. NaOH at

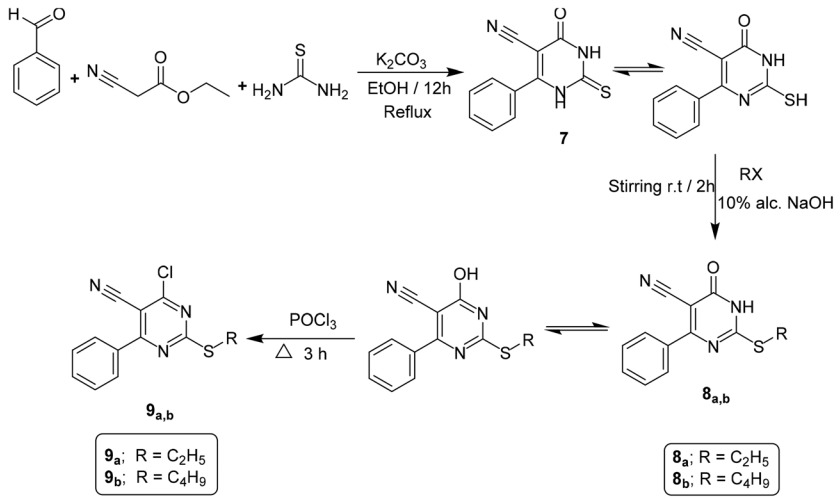

Scheme 1 General procedure for the synthesis of intermediate compounds 7, $\mathbf{8_{a,b}}$, and $\mathbf{9_{a,b}}$.

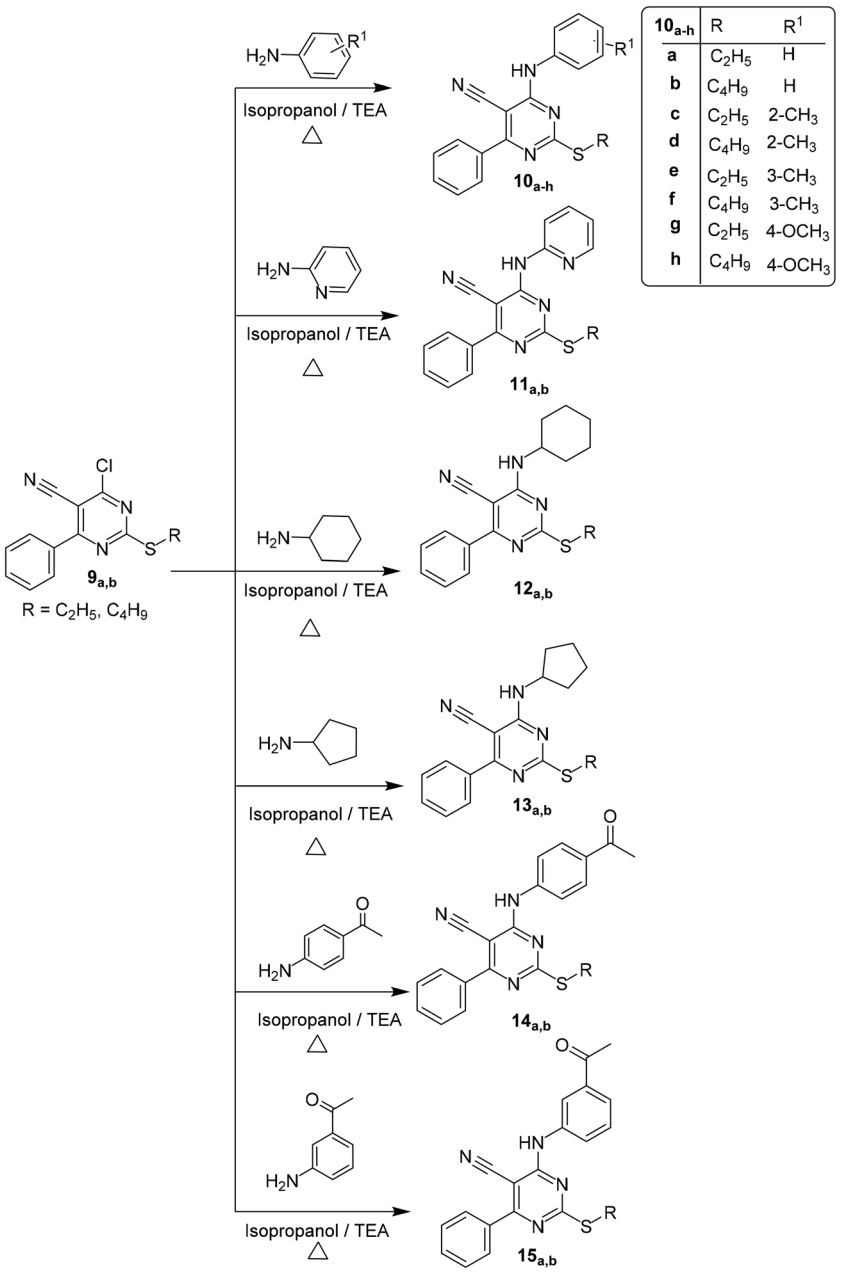

10_{a-h}	R	R^1
a	C_2H_5	H
b	C_4H_9	H
c	C_2H_5	2-CH_3
d	C_4H_9	2-CH_3
e	C_2H_5	3-CH_3
f	C_4H_9	3-CH_3
g	C_2H_5	4-OCH_3
h	C_4H_9	4-OCH_3

Scheme 2 General procedure for the synthesis of target compounds $\mathbf{10_{a-h}}$, $\mathbf{11_{a,b}}$, $\mathbf{12_{a,b}}$, $\mathbf{13_{a,b}}$, $\mathbf{14_{a,b}}$ and $\mathbf{15_{a,b}}$.

room temperature afforded the intermediate, 2-alkylsulfanyl pyrimidine-5-carbonitrile $\mathbf{8_{a,b}}$ which was subsequently chlorinated *via* heating with an excess phosphorus oxychloride in the presence of TEA as an acid binder to obtain the highly reactive intermediate chloro-derivative $\mathbf{9_{a,b}}$ in 75% yield (Scheme 1).

Treating compounds $\mathbf{9_{a,b}}$ with the appropriate aromatic/hetero aromatic amines, cyclic aliphatic amines, phenylhydrazine and/or benzene-sulfonamide derivatives in isopropyl alcohol containing TEA afforded the corresponding final designed compounds (Schemes 2 and 3).

All the synthesized compounds were characterized by ^{1}H and ^{13}C NMR and IR spectroscopy. IR spectra of the designed compounds showed a strong C≡N stretching band around 2206–2218 cm^{-1} and a strong NH absorption band in a range of 3290–3363 cm^{-1}. In addition, all final compounds show strong absorption around 3039–3093 cm^{-1} and 2924–2998 cm^{-1} for aromatic C–H and aliphatic C–H bonds, respectively. Moreover, ^{1}H NMR spectra showed a singlet signal in a range of δ 5.43–10.10 ppm corresponding to the linkage (–NH proton), up-field signals corresponding to the aliphatic protons in a range of δ 0.76–4.67 ppm and down-field signals for some protons in a range of δ 6.93–8.10 ppm, corresponding to the aromatic region. In agreement with the assignments, ^{13}C NMR and APT spectra showed characteristic up-field peaks corresponding to the methyl (CH_3) and methylene

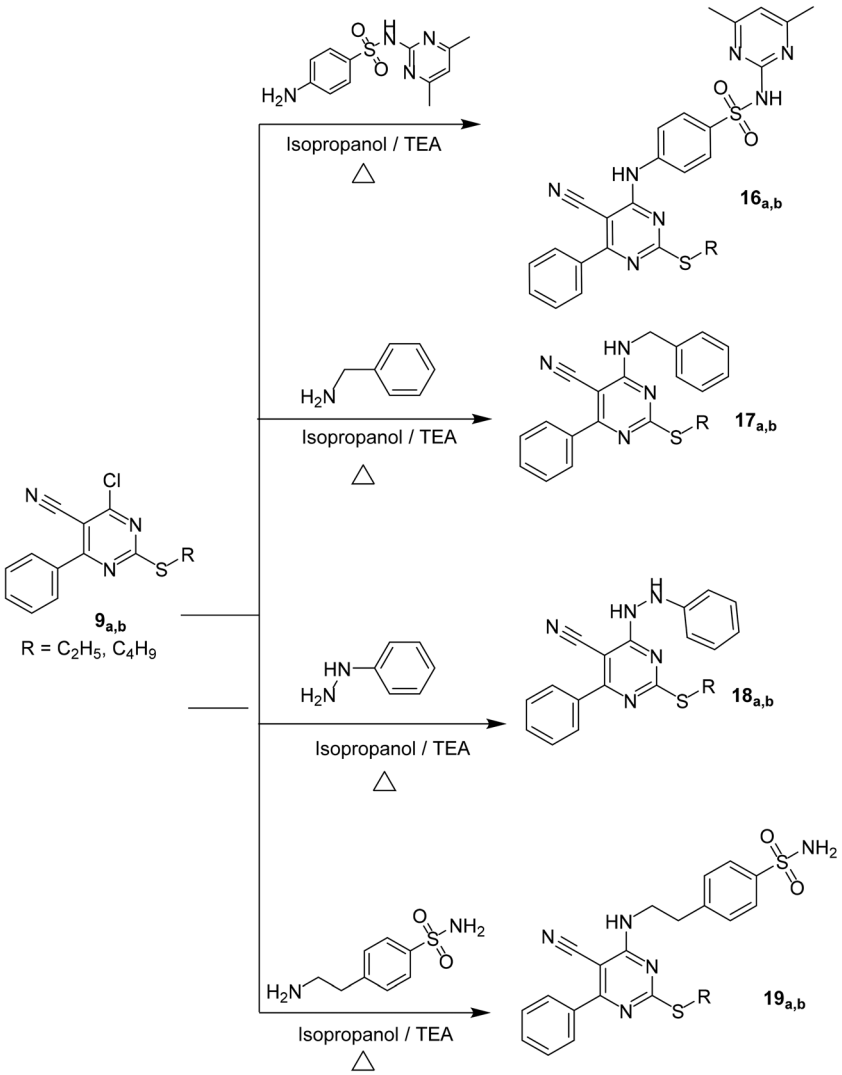

Scheme 3 General procedure for the synthesis of target compounds $16_{a,b}$, $17_{a,b}$, $18_{a,b}$ and $19_{a,b}$.

(CH_2) groups. In addition, ^{13}C NMR and APT spectra showed characteristic peaks for down-field methine (CH) groups.

2.2. Biological evaluation

2.2.1. *In vitro* antiproliferative activities. All the final synthesized (twenty-six) compounds were evaluated for their *in vitro* anti-proliferative activities *via* the standard MTT method,[75–77] against a panel of three human tumor cell lines namely; colorectal carcinoma (HCT-116), hepatocellular carcinoma (HepG-2), and breast cancer (MCF-7). The most active compounds were further evaluated against non-small cell lung cancer cells (A549). MCF-7, HepG-2 and A549 cells have the overexpressed $EGFR^{WT}$.[78–80] Two commercially available drugs (doxorubicin and EGFR inhibitor erlotinib) were used in this test as positive controls. The results were expressed as growth inhibitory concentration (IC_{50}) values and are summarized in Table 1.

The obtained results in Table 1 revealed that the synthesized compounds showed variable antiproliferative activities against the tested cell lines. In general, compounds $\mathbf{10_c}$, $\mathbf{11_a}$, $\mathbf{11_b}$, $\mathbf{12_b}$, $\mathbf{15_b}$, $\mathbf{16_a}$, $\mathbf{17_a}$, and $\mathbf{17_b}$ were more active than the reference drug, erlotinib, against the four tested cell lines. In particular, compound $\mathbf{11_b}$ was found to be the most potent counterpart as it was 5.13, 4.52, 5.72, and 8.37 times more active than erlotinib against HCT-116, HepG-2 MCF-7, and A549 cells, respectively. Also, compound $\mathbf{11_b}$ was more active than doxorubicin against HCT-116, HepG-2, and MCF-7 cells, while compounds $\mathbf{11_a}$ and $\mathbf{12_b}$ were more active than doxorubicin against HepG-2 and MCF-7 cells.

On the other hand, some compounds showed weak antiproliferative activities against all tested cell lines such as compounds $\mathbf{10_e}$, $\mathbf{10_g}$, $\mathbf{10_h}$ and $\mathbf{15_a}$. Finally, compound $\mathbf{10_a}$ was found to be inactive against all tested cell lines, while compound $\mathbf{10_b}$ was inactive against both HCT-116 and MCF-7 (Table 1).

2.2.2. $EGFR^{WT}$ kinase inhibitory assay. The most active candidates ($\mathbf{10_c}$, $\mathbf{10_d}$, $\mathbf{10_f}$, $\mathbf{11_a}$, $\mathbf{11_b}$, $\mathbf{12_b}$, $\mathbf{13_a}$, $\mathbf{13_b}$, $\mathbf{15_b}$, $\mathbf{16_a}$, $\mathbf{17_a}$ and $\mathbf{17_b}$) that showed promising antiproliferative activities

Table 1 *In vitro* anti-proliferative activities towards HCT-116, HepG-2, MCF-7 and A549 cell lines

	IC_{50}[a,d] (μM)			
Comp.	HCT-116	HepG-2	MCF-7	A549
10_a	NA[b]	NA[b]	NA[b]	NT[c]
10_b	NA[b]	45.60 ± 1.82	NA[b]	NT[c]
10_c	13.56 ± 0.54	6.14 ± 0.24	14.49 ± 0.58	8.13 ± 0.32
10_d	18.18 ± 0.73	13.72 ± 0.54	18.53 ± 0.74	12.01 ± 0.48
10_e	41.42 ± 1.66	32.52 ± 1.30	50.57 ± 2.02	NT[c]
10_f	19.01 ± 0.76	21.62 ± 0.86	20.01 ± 0.80	12.76 ± 0.51
10_g	44.44 ± 1.78	39.64 ± 1.58	46.59 ± 1.86	NT[c]
10_h	41.76 ± 1.67	32.34 ± 1.29	39.97 ± 1.60	NT[c]
11_a	6.56 ± 0.26	3.89 ± 0.04	8.00 ± 0.32	3.71 ± 0.14
11_b	3.37 ± 0.13	3.04 ± 0.12	4.14 ± 0.16	2.40 ± 0.09
12_a	16.78 ± 0.67	12.37 ± 0.49	30.13 ± 1.21	NT[c]
12_b	6.79 ± 0.27	6.27 ± 0.25	8.64 ± 0.34	4.88 ± 0.19
13_a	15.84 ± 0.63	14.08 ± 0.56	20.95 ± 0.84	11.12 ± 0.44
13_b	19.29 ± 0.77	16.36 ± 0.65	21.16 ± 0.84	11.80 ± 0.47
14_a	27.69 ± 1.11	25.39 ± 1.01	32.84 ± 1.31	NT[c]
14_b	38.20 ± 1.52	28.02 ± 1.12	48.44 ± 1.94	NT[c]
15_a	58.27 ± 2.33	43.44 ± 1.74	55.19 ± 2.21	NT[c]
15_b	9.29 ± 0.37	10.18 ± 0.41	12.09 ± 0.48	9.77 ± 0.39
16_a	9.71 ± 0.38	8.22 ± 0.33	17.85 ± 0.71	6.22 ± 0.23
16_b	19.05 ± 0.76	12.04 ± 0.48	17.17 ± 0.68	NT[c]
17_a	12.55 ± 0.50	9.20 ± 0.37	13.62 ± 0.54	8.45 ± 0.34
17_b	13.08 ± 0.52	9.90 ± 0.39	17.48 ± 0.69	8.14 ± 0.32
18_a	23.57 ± 0.94	18.16 ± 0.73	24.81 ± 0.99	NT[c]
18_b	36.21 ± 1.45	29.85 ± 1.19	34.24 ± 1.37	NT[c]
19_a	33.05 ± 1.32	28.05 ± 1.22	40.49 ± 1.62	NT[c]
19_b	32.99 ± 1.31	29.29 ± 1.17	39.64 ± 1.58	NT[c]
Doxorubicin	5.72 ± 0.22	6.96 ± 0.27	8.65 ± 0.34	NT[c]
Erlotinib	17.32 ± 1.77	13.76 ± 1.31	23.70 ± 1.92	20.11 ± 1.92

[a] IC_{50} values are the mean ± S.D. of three separate experiments. [b] NA: Compounds having IC_{50} values >50 μM. [c] NT: Compounds not tested for their anti-proliferative activities. [d] IC_{50} (μM): 1–10 (very strong), 11–20 (strong), 21–30 (moderate), and 31–50 (weak).

against the tested cell lines were subjected to further investigation for their $EGFR^{WT}$ kinase inhibitory activities. Homogeneous time resolved fluorescence (HTRF) assay[81] was applied in this test, using erlotinib as a reference standard (Table 2).

In general, all the tested compounds could interfere with the $EGFR^{WT}$ activity with IC_{50} values ranging from 0.09 to 6.64 μM. In particular, compounds **11_a** and **11_b** exhibited stronger activities than erlotinib (IC_{50} = 0.31 μM) with IC_{50} values of 0.25 and 0.09 μM, respectively, whereas, compounds **10_c** and **10_d**, and **12_b** showed comparable activities with erlotinib with IC_{50} values of 0.50, 0.41, and 0.68 μM, respectively. On the other hand, compounds **10_f**, **13_a**, **13_b**, **15_b**, **16_a**, **17_a**, and **17_b** showed moderate activities against $EGFR^{WT}$ with IC_{50} values ranging from 0.82 to 6.64 μM.

2.2.3. $EGFR^{T790M}$ kinase inhibitory assay. Furthermore, the most active cytotoxic compounds (**10_c**, **10_d**, **10_f**, **11_a**, **11_b**, **12_b**, **13_a**, **13_b**, **15_b**, **16_a**, **17_a** and **17_b**) were also further evaluated for their inhibitory activities against mutant $EGFR^{T790M}$. Gefitinib was tested as a positive control.

In general, most of the synthesized compounds could interfere with the $EGFR^{T790M}$ activity, exhibiting stronger activities than gefitinib such as compounds **10_c**, **11_a**, **11_b**, **12_b**, **16_a**, **17_a** and **17_b** with IC_{50} values ranging from 4.03 to 16.97 μM. In particular, compound **11_b** (IC_{50} = 4.03 μM) was found to be the most potent counterpart as it was 5.43 times more active than gefitinib (IC_{50} = 21.91 μM), while compounds **13_a**, **13_b**, and **15_b** showed comparable inhibitory activities to gefitinib with IC_{50} values of 24.59, 24.22, and 20.66 μM, respectively. On the other hand, compounds **10_d** and **10_f** showed weak activities when compared with the reference drug with IC_{50} values of 30.35 and 46.51 μM, respectively (Table 2).

Table 2 *In vitro* enzymatic inhibitory activities of the target compounds against $EGFR^{WT}$ and $EGFR^{790M}$

Comp.	$EGFR^{WT}$ IC_{50}[a] (μM)	$EGFR^{T790M}$ IC_{50}[a] (μM)
10_c	0.50 ± 0.02	10.85 ± 0.43
10_d	0.41 ± 0.16	30.35 ± 1.21
10_f	6.64 ± 0.26	46.51 ± 1.86
11_a	0.25 ± 0.01	8.24 ± 0.33
11_b	0.09 ± 0.04	4.03 ± 0.16
12_b	0.68 ± 0.03	8.40 ± 0.34
13_a	4.77 ± 0.19	24.59 ± 0.98
13_b	4.87 ± 0.19	24.22 ± 0.97
15_b	4.29 ± 0.17	20.66 ± 0.83
16_a	3.05 ± 0.12	14.37 ± 0.57
17_a	0.82 ± 0.03	16.97 ± 0.68
17_b	3.92 ± 0.16	15.35 ± 0.61
Erlotinib	0.31 ± 0.11	NT[b]
Gefitinib	NT[b]	21.91 ± 0.88

[a] Data were expressed as mean ± standard error (S.E.) of three independent experiments. [b] NT: Compounds not tested.

2.2.4. Structure–activity relationships (SAR). As outlined in the rationale for the molecular design, we aimed at studying the SAR of the newly synthesized compounds as potential anticancer agents.

Firstly, the effect of substitution on the 2-mercapto group by different alkyl moieties has been explored. The decreased IC_{50} values of compounds **11_b** and **12_b** incorporating butyl side chains compared to the corresponding members incorporating ethyl ones **11_a** and **12_a** indicated that substitution with a long chain aliphatic group is preferred over incorporating a shorter chain.

We then investigated the impact of the linker length on the cytotoxicity of the synthesized compounds. A comparison of the activities of compounds **$10_{a,b}$** (with an NH linker), **$17_{a,b}$** (with an NH-CH_2 linker), **$18_{a,b}$** (with an NHNH linker), and **$19_{a,b}$** (with an $NHCH_2CH_2$ linker) indicated that the activities decreased in the order of NH-CH_2 linker > NHNH linker > $NHCH_2CH_2$ linker > NH linker.

Next, the effect of the hydrophobic head on the activity was analyzed. The heterocyclic moiety (compounds **$11_{a,b}$**) had a greater cytotoxic effect than alicyclic moieties (compounds **$12_{a,b}$** and **$13_{a,b}$**), which were more effective than non-heteroaromatic structures (compounds **$10_{a,b}$**). In addition, the six-membered alicyclic moiety (compounds **$12_{a,b}$**) showed a greater effect than the five-membered one (compounds **$13_{a,b}$**).

Finally, the effect of the substitutions on the phenyl ring of the hydrophobic head was investigated. The decreased IC_{50} values of compounds **$14_{a,b}$** incorporating electron withdrawing

(acetyl) groups compared to compounds $\mathbf{10_{c-f}}$ incorporating electron donating (methyl and methoxy) groups indicated that electron withdrawing derivatives were more advantageous than electron donating ones.

2.2.5. Correlation of cytotoxicity with EGFR^{WT} inhibition. As we reported, the tested compounds can inhibit EGFR^{WT} in the tested cell lines. Next, we tested whether the EGFR^{WT} inhibition can lead to cell death. To confirm this, the activities of the studied compounds as EGFR^{WT} inhibitors were plotted against their corresponding cytotoxicity in a simple linear regression setting for the cell lines used in this study. The obtained coefficients of determination (R^2) imply the correlation between EGFR^{WT} inhibition and the induced cytotoxicity. The R^2 values for HCT-116, HepG-2, MCF-7, and A549 were 0.32 (P value: 0.05245), 0.6376 (P value: 0.0018), 0.4795 (P value: 0.0126) and 0.4398 (P value: 0.0187), respectively (Fig. 6).

2.2.6. Cell cycle analysis. The effect of the most active compound $\mathbf{11_b}$ on the cell cycle distribution and apoptosis induction was evaluated using HCT-116, HepG-2, and MCF-7 cells according to the procedure described by Wang *et al.*[82] The HCT-116, HepG-2, and MCF-7 cells were incubated with compound $\mathbf{11_b}$ for 24 h at concentrations equal to its IC_{50} against the three cell lines (3.37, 3.04, and 4.14 μM, respectively). Then, the effect of compound $\mathbf{11_b}$ on the cell cycle profile was analyzed.

The results revealed that exposure of HCT-116 cells to compound $\mathbf{11_b}$ led to an interference with the normal cell cycle distribution of this cell line. This compound induced a significant increase in the percentage of cells at pre-G_1 phases (which could be indicative of apoptosis) and G_2-M phases by 5.4 and 1.5 fold, respectively, compared to the control. With regard to HepG-2 cells, compound $\mathbf{11_b}$ induced an increase in the percentage of cells at pre-G_1 phases and G_2-M phases by 6.7 and 1.6 fold, respectively, compared to the control. For MCF-7 cells, compound $\mathbf{11_b}$ induced an increase in the percentage of cells at pre-G_1 phases and G_2-M phases by 4.4 and 1.5 fold, respectively, compared to the control. These results clearly indicated that compound $\mathbf{11_b}$ arrests the G_2-M phase of the cell cycle (Table 3 and Fig. 7, 8).

2.2.7. Annexin V-FITC apoptosis assay. In order to confirm the apoptosis induction on HCT-116, HepG-2, and MCF-7 cells by compound $\mathbf{11_b}$, Annexin V and PI double staining assay with FITC was used[83] to explore the mode of induced cell death. HCT-116, HepG-2, and MCF-7 cells were incubated with $\mathbf{11_b}$ at concentrations of 3.37, 3.04, and 4.14 μM, respectively, for 24 h. The obtained results are represented in Table 4 and Fig. 9 and 10.

The results revealed that the application of compound $\mathbf{11_b}$ on HepG-2 cells increases the early apoptosis ratio (lower right quadrant of the cytogram) from 0.61% to 5.98%, and increases the late apoptosis ratio (upper right quadrant of the cytogram)

Table 3 Effect of compound $\mathbf{11_b}$ on cell cycle progression of HCT-116, HepG-2, and MCF-7 cells

	Cell cycle distribution (%)			
Sample	%G0–G1	%S	%G2-M	%Pre-G1
$\mathbf{11_b}$/HCT-116	47.44	30.17	22.39	13.74
Cont. HCT-116	52.74	32.28	14.98	2.53
$\mathbf{11_b}$/HepG-2	40.23	35.11	24.66	15.82
Cont. HepG-2	55.31	29.44	15.25	2.37
$\mathbf{11_b}$/MCF-7	46.3	33.09	20.61	11.86
Cont. MCF-7	57.11	29.42	13.47	2.70

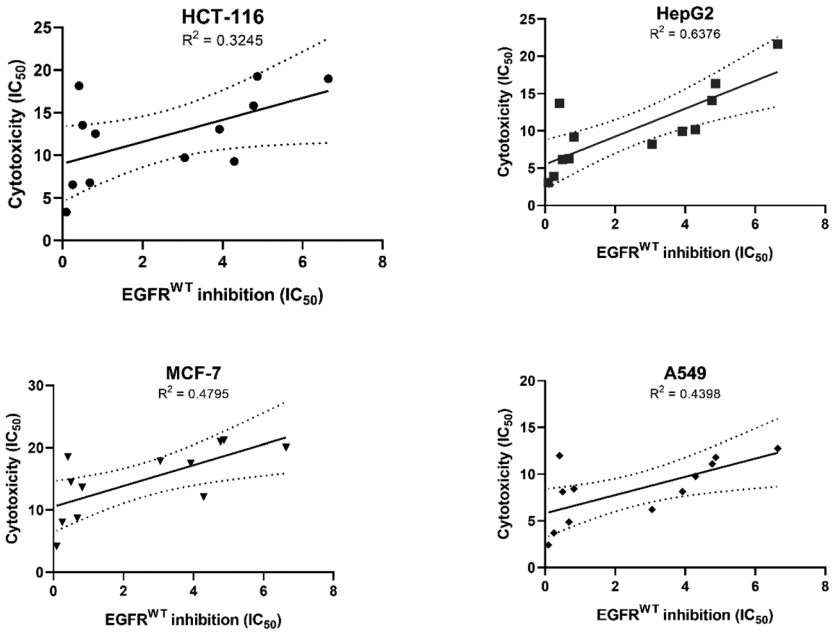

Fig. 6 Correlation of cytotoxicity with EGFR^{WT} inhibition on four cell line models HCT-116, HepG-2, MCF-7, and A549.

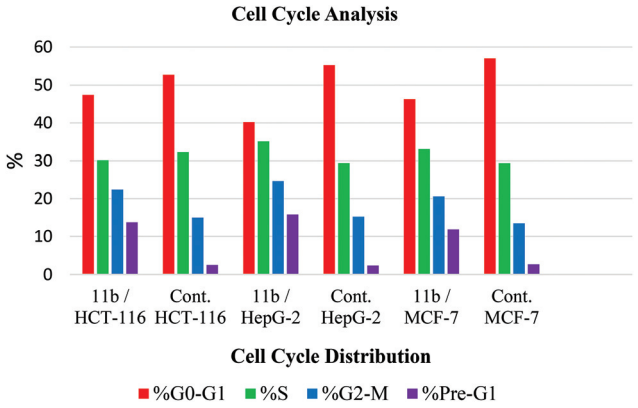

Fig. 7 Percentage of induced cell death by compound **11b** on HCT-116, HepG-2, and MCF-7 cells.

from 0.54% to 5.13%. This means that compound **11b** induced almost up to 9-folds for both early and late cellular apoptosis when compared with the control. For HepG-2 cells, compound

Table 4 Apoptosis and necrosis percent induced by compound **11b**

	Apoptosis			
Sample	Total	Early	Late	Necrosis
11b/HCT-116	13.74	5.98	5.13	2.63
Cont. HCT-116	2.53	0.61	0.54	1.38
11b/HepG-2	15.82	7.54	5.52	2.76
Cont. HepG-2	2.37	0.59	0.47	1.31
11b/MCF-7	11.86	4.19	5.08	2.59
Cont. MCF-7	2.7	0.68	0.57	1.45

11b increased the early apoptosis ratio from 0.59% to 7.54%, and the late apoptosis ratio from 0.47% to 5.52%. This means that compound **11b** induced almost up to 12-folds for both early and late cellular apoptosis when compared with the control. For MCF-7 cells, compound **11b** increased the early apoptosis ratio from 0.68% to 4.19%, and the late apoptosis ratio from 0.57% to 5.08%. This means that compound **11b** induced almost up to 7-folds for both early and late cellular apoptosis when compared with the control. These data indi-

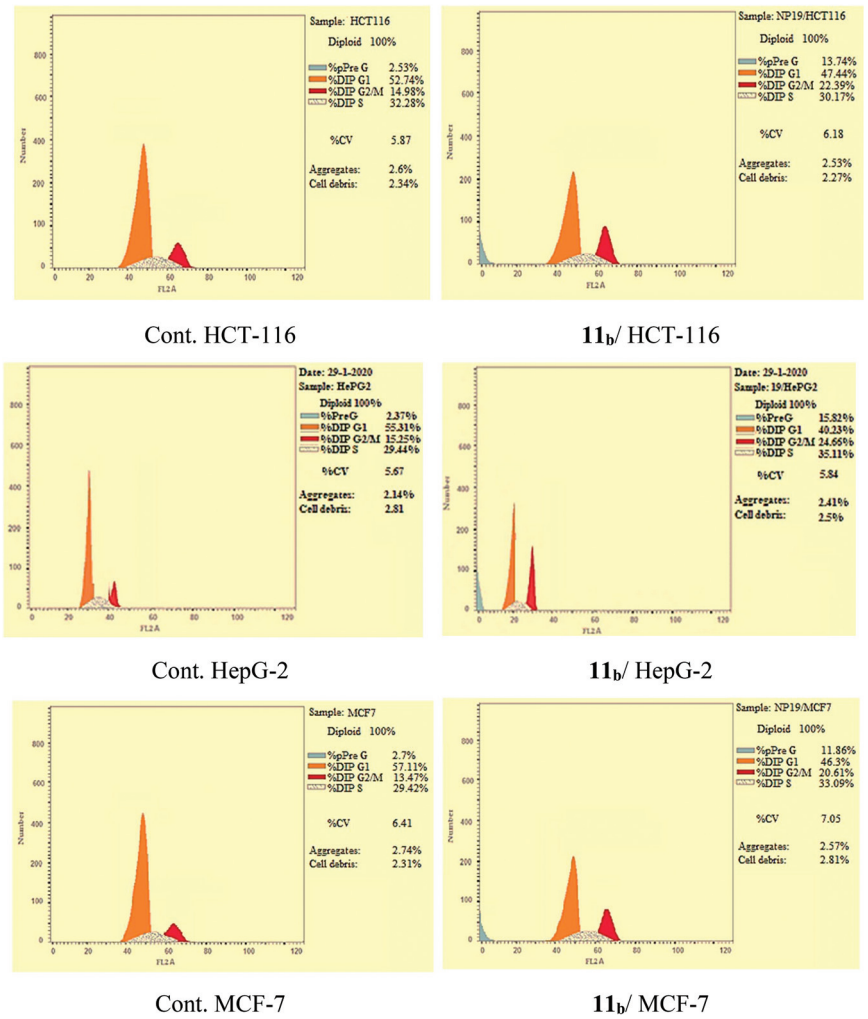

Fig. 8 HCT-116, HepG-2, and MCF-7 cell distribution upon treatment with compound **11b**.

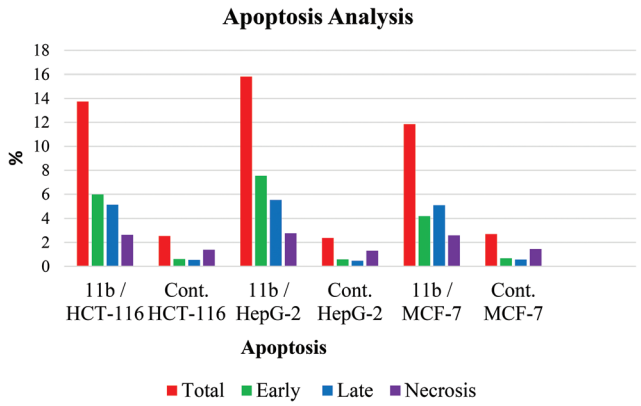

Fig. 9 Apoptosis effect of compound $\mathbf{11_b}$ on HCT-116, HepG-2, and MCF-7 cells.

cate that compound $\mathbf{11_b}$ shows a potent apoptotic effect against HCT-116, HepG-2, and MCF-7 cells.

2.2.8. Caspase-3 determination. Caspases, a family of cysteine-dependent aspartate-directed proteases, are prominent among the death proteases. Regulation of caspase activation and activity occurs at several different levels.[84] In apoptosis, activation of caspases turns off a number of signals and leads to eventual cell death.[85] EGFR signaling serves as one of the critical survival signals, which may become the target of caspase activation, in order to ensure the execution of apoptosis.[86] The EGFR is down-regulated in response to apoptosis by a few treatments. It has been reported that caspase-3 specifically cleaves and inactivates the EGFR.[87,88]

To analyze the effect of compound $\mathbf{11_b}$ on the levels of caspase-3, HepG-2 cells were treated with such a compound at a concentration of 3.04 μM for 24 h. The results revealed that it produced a marked increase in the level of caspase-3 (358.19 pg mL^{-1}, 6.5 fold) compared to the control cells (55.27 pg mL^{-1}) (Table 5 and Fig. 11).

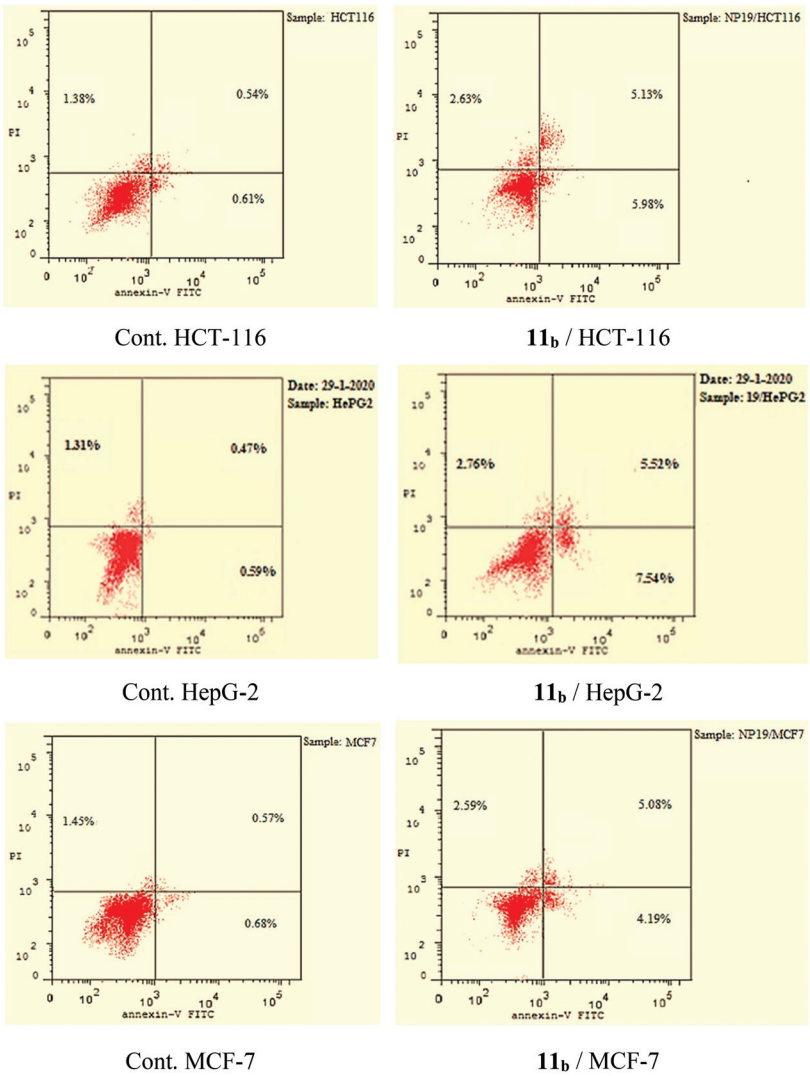

Fig. 10 Apoptosis and necrosis percent induced by compound $\mathbf{11_b}$.

Table 5 Effect of compound 11_b on active caspase-3 in HepG-2 cells after 24 h treatment

Sample	Caspase-3[a] (pg mL^{-1})
Cont. HepG-2	55.27 ± 2.21
Compound 11_b/HepG-2	358.19 ± 20.87

[a] Values are given as mean ± SEM of three independent experiments.

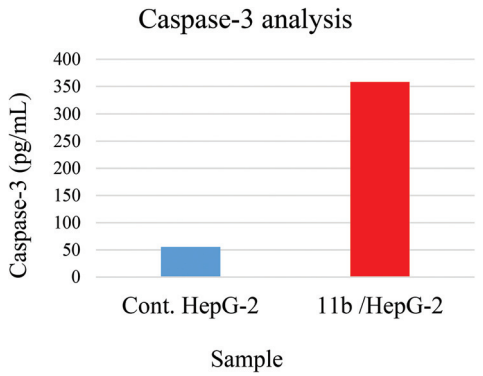

Fig. 11 Graphical representation for active caspase-3 assay of compounds 11_b. The data are presented as the mean ± SEM from three independent experiments.

Table 6 The docking binding free energies of the synthesized compounds against EGFR^{WT} and EGFR^{T790M}

Comp.	Binding free energy (kcal mol^{-1}) EGFR^{WT}	EGFR^{T790M}
10_a	−6.93	−5.91
10_b	−6.90	−6.28
10_c	−6.98	−6.33
10_d	−7.30	−6.00
10_e	−7.03	−5.71
10_f	−7.34	−6.72
10_g	−7.41	−6.67
10_h	−7.64	−6.15
11_a	−6.57	−6.14
11_b	−7.22	−6.88
12_a	−6.77	−6.12
12_b	−7.24	−6.53
13_a	−6.00	−6.27
13_b	−7.21	−6.54
14_a	−7.59	−6.31
14_b	−8.16	−6.53
15_a	−7.42	−6.59
15_b	−7.99	−6.21
16_a	−8.66	−7.32
16_b	−9.55	−6.74
17_a	−7.05	−6.06
17_b	−7.36	−6.07
18_a	−7.31	−5.98
18_b	−7.28	−6.00
19_a	−7.90	−6.82
19_b	−7.26	−6.64
Erlotinib	−7.55	—
TAK-285	—	−7.11

2.3. *In silico* studies

2.3.1. Docking studies. Docking studies were carried out for the synthesized compounds against the ATP binding sites of EGFR-TK Wild-type (EGFR^{WT}, PDB: 4HJO)[89] and EGFR-TK mutant type (EGFR^{T790M}, PDB: 3W2O)[90] to examine the mode of binding with the proposed target. The results of docking studies revealed that the docked compounds have good binding affinities against EGFR^{WT} with binding free energies ranging from −6.77 to −9.55 kcal mol^{-1} (Table 6).

A molecular docking protocol was implemented using the MOE 14.0 software. The target proteins were prepared and the active binding sites identified based on the positional coordinates of the co-crystallized inhibitors. The results of the docking protocol were validated by re-docking of the co-crystallized ligands (erlotinib and TAK-285) inside the active sites of EGFR^{WT} and EGFR^{T790M}, respectively. The root mean square deviations (RMSD) between the re-docked conformers and the co-crystallized conformers of erlotinib and TAK-285 were 1.5 and 0.90, respectively, which confirms the validity of the docking protocol (Fig. 12).

Erlotinib, as a co-crystallized ligand, showed a binding energy of −7.55 kcal mol^{-1}. In detail, the quinazoline moiety occupied the adenine pocket of EGFR^{WT}, where the pyrimidine ring formed one hydrogen bond with Met769 with a distance of 2.22 Å. The phenyl ring of the quinazoline moiety was incorporated in pi-Sigma interactions with Lue694 and Leu820. The terminal ethynylphenyl moiety was embedded in the hydrophobic pocket I creating hydrophobic interactions with Lys721, Val702, and Ala719 residues. Additionally, the hydrophobic region II was occupied by the two 2-methoxyethoxy groups forming hydrophobic interactions with Gly772 and Leu694 residues and one hydrogen bond with Cys773 (Fig. 13).

Compound 11_b as a representative example exhibited a binding mode similar to that of the reference ligand, erlotinib. It gave an affinity value of −7.22 kcal mol^{-1}. The pyrimidine-5-carbonitrile moiety was lodged in the adenine pocket of the EGFR^{WT} forming hydrophobic interactions with Val702 and Lys721. The nitrile group formed a hydrogen bond with Thr766 with a distance of 2.02 Å. The 2-pyridyl group occupied the hydrophobic pocket I forming a hydrophobic interaction with Leu764. In addition, the N-atom of the pyridine moiety formed a hydrogen bond with Thr830 with a distance of 2.23 Å. Such extra hydrogen bonding interactions may explain the higher activity of this compound compared to that of the corresponding members. Moreover, the phenyl group at position-4 occupied the hydrophobic region II forming a hydrophobic interaction with Ala719. The sulfur atom formed one hydrogen bond with Lys721 with a distance of 2.90 Å (Fig. 14). The binding mode of compound 16_b against EGFR^{WT} (as another example) is illustrated in the ESI†.

The results of docking studies revealed that the docked compounds have good binding affinities against EGFR^{T790M} with binding free energies ranging from −16.90 to −26.96 kcal mol^{-1} (Table 6). TAK-285, as a co-crystallized ligand, showed a binding energy of −7.11 kcal mol^{-1}. In detail, the pyrrolo[3,2-*d*]pyrimidine moiety occupied the adenine

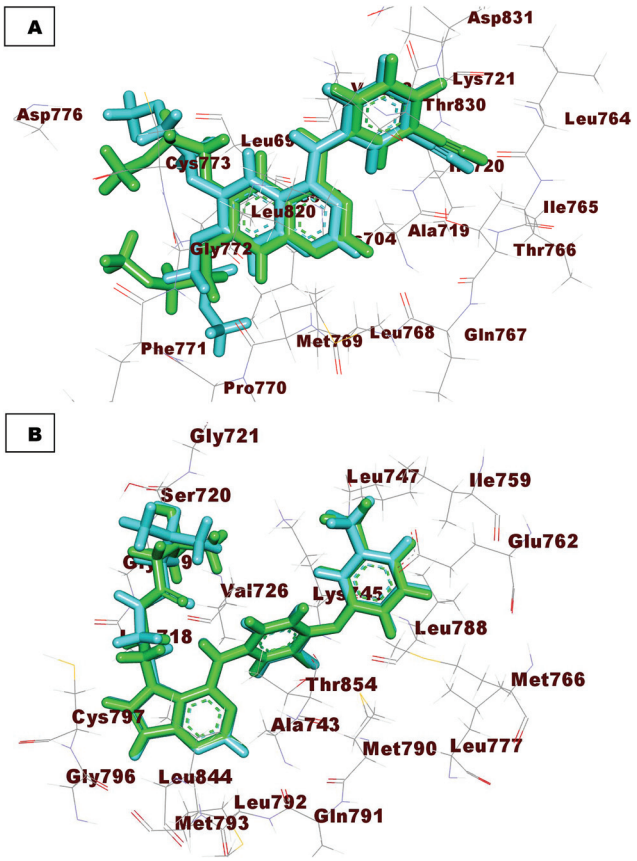

Fig. 12 (A) and (B) 3D images of the superimposition of the re-docked conformers of erlotinib and TAK-285 (turquoise) over the co-crystallized conformers (green) with RMSD values of 1.5 and 0.90, respectively.

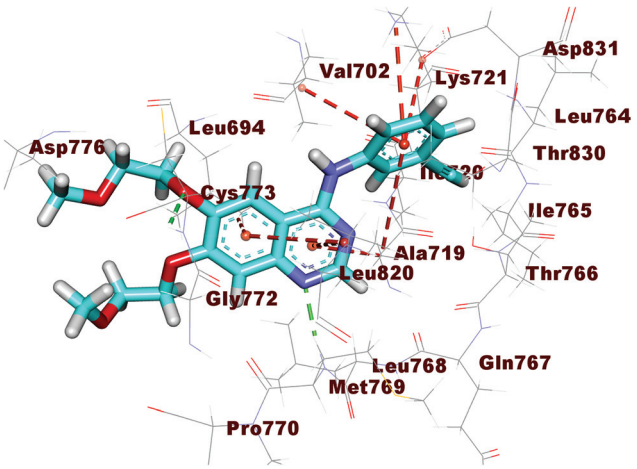

Fig. 13 Erlotinib docked into the active site of $EGFR^{WT}$. The hydrogen bonds are represented in green dashed lines. The pi interactions are represented in orange lines.

pocket of $EGFR^{T790M}$. It formed hydrophobic interactions with Ala743 and Leu844. The pyrimidine moiety formed one hydrogen bond with Met793 with a distance of 2.23 Å. The terminal 3-(trifluoromethyl)phenoxy group was embedded in the hydrophobic pocket I creating hydrophobic interactions with Lys745 and Ile759. The trifluoromethane group formed a hydrogen bond with Lys745 with a distance of 1.41 Å. Additionally, the hydrophobic region II was occupied by the *N*-ethyl-3-hydroxy-3-methylbutanamide moiety forming hydrogen bonds with Ser720 with a distance of 1.79 Å. The central phenyl moiety

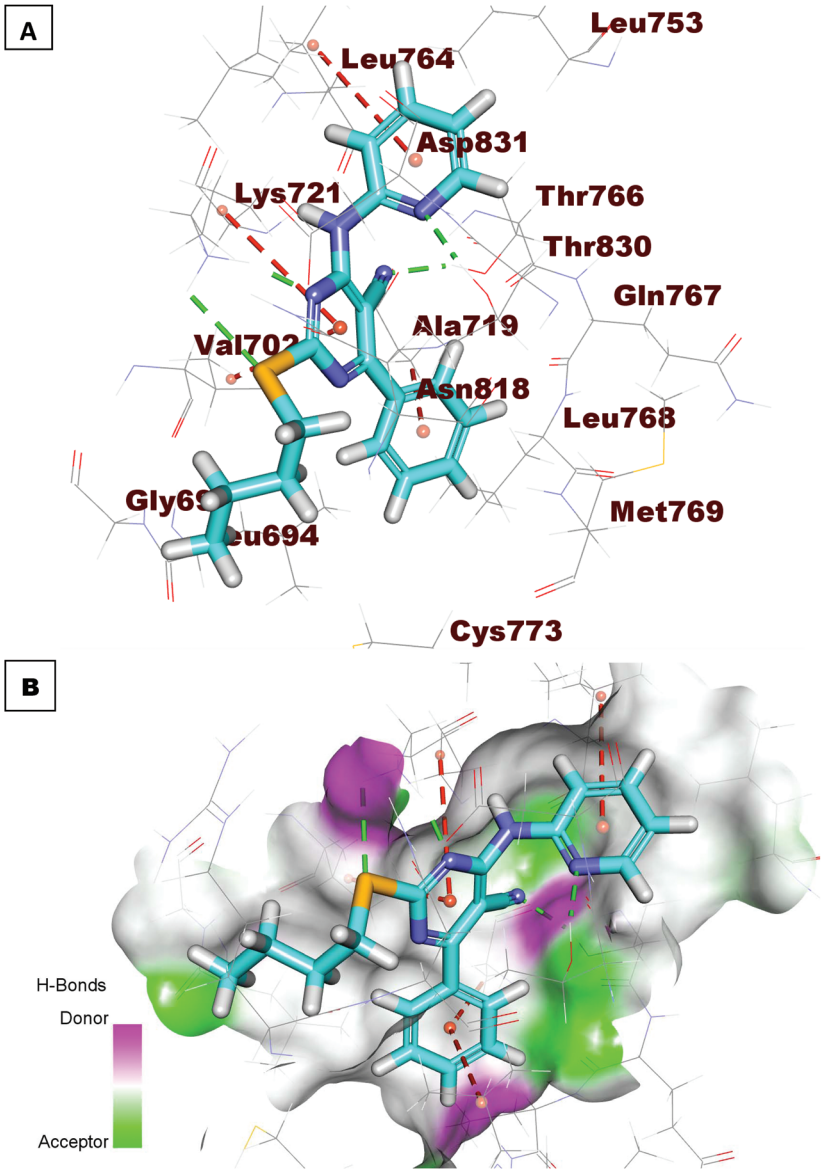

Fig. 14 (A) Compound $\mathbf{11_b}$ docked into the active site of $EGFR^{WT}$. The hydrogen bonds are represented in green dashed lines. The pi interactions are represented in orange lines. (B) Mapping surface showing compound $\mathbf{11_b}$ occupying the active pocket of $EGFR^{WT}$.

formed pi-Sigma interactions with Met790, Val726, and Lys745 (Fig. 15).

Compound $\mathbf{11_b}$ exhibited a binding mode similar to that of TAK-285 with an affinity value of −6.88 kcal mol^{-1}. The pyrimidine-5-carbonitrile moiety was embedded in the adenine pocket of $EGFR^{WT}$ forming hydrophobic interactions with Lys745, Val726, and Ala743. The 2-pyridyl group occupied the hydrophobic pocket I forming a hydrogen bonding interaction with Lys745. The hydrogen bonding interaction between the pyridine moiety and Lys745 may increase the binding affinity of compound $\mathbf{11_b}$ toward the receptor, and consequently increases its inhibitory activity compared to the corresponding members. Moreover, the phenyl group at position-4 occupied the hydrophobic region II forming hydrophobic interactions with Ala743 and Leu844. The butyl moiety formed three hydrophobic interactions with Ile759, Leu788, and Lys745 (Fig. 16). The binding mode of compound $\mathbf{16_b}$ against $EGFR^{T790M}$ (as another example) is illustrated in the ESI.†

2.3.2. *In silico* ADMET analysis. ADMET studies were carried out for the most cytotoxic members $\mathbf{10_c}$, $\mathbf{10_d}$, $\mathbf{10_f}$, $\mathbf{11_a}$, $\mathbf{11_b}$, $\mathbf{12_b}$, $\mathbf{13_a}$, $\mathbf{13_b}$, $\mathbf{15_b}$, $\mathbf{16_a}$, $\mathbf{17_a}$, and $\mathbf{17_b}$. Erlotinib and gefitinib were used as reference compounds. ADMET studies include many descriptors. (i) Blood brain barrier penetration which predicts the blood brain barrier penetration of a molecule. (ii) Intestinal absorption which predicts human intestinal absorption (HIA) after oral administration. (iii) Aqueous solubility which predicts the solubility of each compound in water at 25 °C. (iv) CYP2D6 binding which predicts cytochrome P450 2D6 enzyme inhibition. (v) Plasma protein binding which predicts the fraction of the drug bound to plasma proteins in

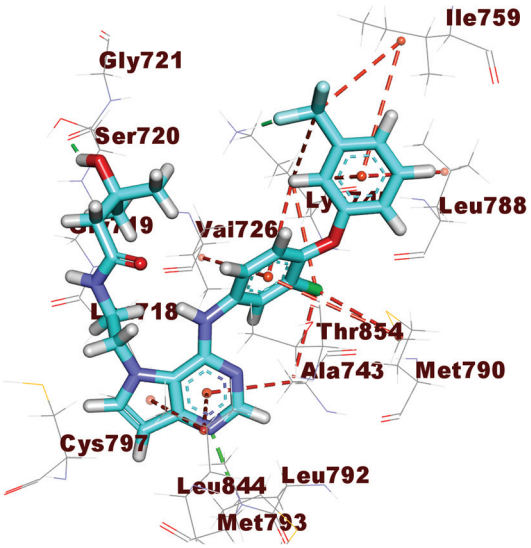

Fig. 15 Co-crystallized ligand (TAK-285) docked into the active site of $EGFR^{T790M}$. The hydrogen bonds are represented in green dashed lines.

blood.[91] Discovery studio 4.0 was used to predict ADMET descriptors for all compounds. The predicted descriptors are listed in Table 7.

ADMET–Blood Brain Barrier (BBB) penetration studies predicted that the BBB penetration levels of most of the compounds ($\mathbf{10_d}$, $\mathbf{10_f}$, $\mathbf{11_b}$, $\mathbf{12_b}$, $\mathbf{13_b}$, $\mathbf{15_b}$, $\mathbf{16_a}$, and $\mathbf{17_b}$) are very low. Accordingly, such compounds were expected to be safe to the CNS. On the other hand, compound $\mathbf{10_c}$ was predicted to have a high BBB penetration level and compounds $\mathbf{11_a}$, $\mathbf{13_a}$, and $\mathbf{17_a}$ showed high BBB penetration levels. All the tested compounds showed low to very low range levels of ADMET aqueous solubility. Intestinal absorption is defined as a percentage of the absorbed compound from the gut wall.[92] A well-absorbed compound is one that is absorbed at least 90% into the bloodstream in humans.[93] According to our ADMET studies, absorption levels of compounds $\mathbf{10_c}$, $\mathbf{11_a}$, $\mathbf{11_b}$, $\mathbf{12_b}$, $\mathbf{13_a}$, $\mathbf{13_b}$, $\mathbf{15_b}$, $\mathbf{17_a}$, and $\mathbf{17_b}$ appeared in the good and moderate range, while compounds **10d**, **10f**, and **16a** showed poor intestinal absorption.

The cytochrome P450 2D6 (CYP2D6) model predicts CYP2D6 enzyme inhibition using a 2D chemical structure as the input. CYP2D6 is involved in the metabolism of a wide range of substrates in the liver and its inhibition by a drug constitutes a majority cases of drug–drug interactions. Therefore, a CYP2D6 inhibition experiment is required as part of the regulatory procedures in the drug discovery and development process.[94] All examined members were predicted as non-inhibitors of CYP2D6 except compound $\mathbf{17_b}$. Consequently, a liver dysfunction side effect is not expected upon administration of these compounds. The plasma protein binding model predicts whether a compound is likely to be highly bound (≥90% bound) to carrier proteins in blood.[95] All compounds are expected to bind plasma protein more than 90% except compound $\mathbf{16_a}$ (Fig. 17) (ESI†).

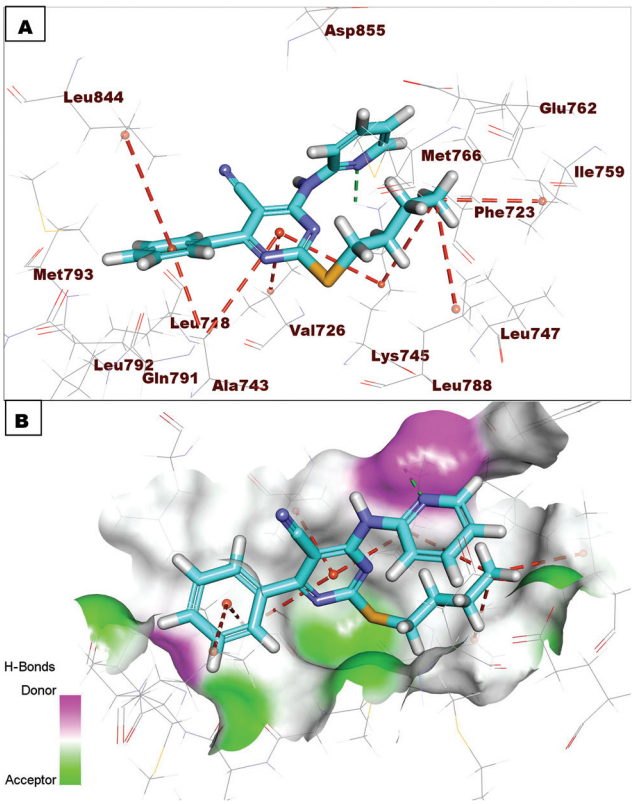

Fig. 16 (A) Binding of compound $\mathbf{11_b}$ with $EGFR^{T790M}$. The hydrogen bonds are represented in green dashed lines and the pi interactions are represented in orange dashed lines. (B) Mapping surface showing compound $\mathbf{11_b}$ occupying the active pocket of $EGFR^{T790}$.

Table 7 Predicted ADMET for the designed compounds and reference drugs

Comp.	BBB level[a]	Solubility level[b]	Absorption level[c]	CYP2D6 prediction[d]	PPB prediction[e]
10_c	0	1	1	False	True
10_d	4	1	2	False	True
10_f	4	1	2	False	True
11_a	1	2	0	False	True
11_b	4	1	1	False	True
12_b	4	1	1	False	True
13_a	1	2	0	False	True
13_b	4	1	1	False	True
15_b	4	1	1	False	True
16_a	4	1	2	False	False
17_a	1	2	0	False	True
17_b	4	1	1	True	True
Erlotinib	1	2	0	False	True
Gefitinib	2	2	0	False	True

[a] BBB level, blood brain barrier level: 0 = very high, 1 = high, 2 = medium, 3 = low, and 4 = very low. [b] Solubility level, 1 = very low, 2 = low, 3 = good, and 4 = optimal. [c] Absorption level, 0 = good, 1 = moderate, 2 = poor, and 3 = very poor. [d] CYP2D6 = cytochrome P2D6, TRUE = inhibitor, and FALSE = non inhibitor. The classification whether a compound is a CYP2D6 inhibitor using a cutoff Bayesian score of 0.161. [e] PBB, plasma protein binding, FALSE means less than 90%, and TRUE means more than 90%. The classification whether a compound is highly bound (≥90% bound) to plasma proteins using a cutoff Bayesian score of −2.209.

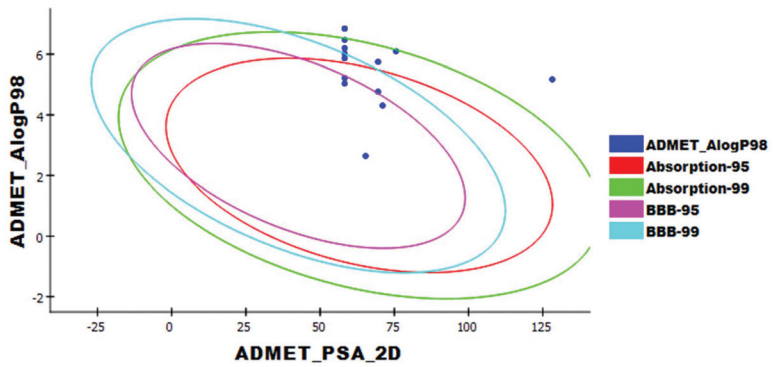

Fig. 17 The expected ADMET study.

3. Conclusion

A series of EGFR inhibitors was designed, synthesized and evaluated for antiproliferative activities against HCT-116, HepG-2, MCF-7, and A549 cell lines. Compound **11_b** (IC_{50} = 3.37, 3.04, 4.14, and 2.40 μM) was found to be the most potent counterpart as it was 5.13, 4.52, 5.72, and 8.37 times more active than erlotinib (IC_{50} = 17.32, 13.76, 23.70, and 20.11 μM) against HCT-116, HepG-2, MCF-7, and A549 cells, respectively. The inhibitory profiles against two isoforms: $EGFR^{WT}$ and $EGFR^{T790M}$ were assessed for the most promising candidates (**10_c, 10_d, 10_f, 11_a, 11_b, 12_b, 13_a, 13_b, 15_b, 16_a, 17_a** and **17_b**). The tested compounds showed promising activities against both wild type and mutant forms, and compound **11_b** emerged as the most potent EGFR inhibitor with IC_{50} values of 0.09 and 4.03 μM against $EGFR^{WT}$ and $EGFR^{T790M}$, respectively. In order to get an additional comprehension about the effect of the synthesized compounds on the inhibition of cancer cell growth, the effect of compound **11_b** on cell cycle distribution and apoptosis induction was analyzed. Compound **11_b** induced apoptosis based on annexin V staining and arrested the cell cycle at the G2/M phase. Structure–activity relationship studies revealed that hydrophobic heterocyclic moieties had a greater cytotoxic effect than alicyclic moieties, which were more effective than non-hetero-aromatic structures, and that the cytotoxic effects correlated with EGFR-inhibitory effects. To further understand and rationalize the strong inhibitory profile of the compounds against $EGFR^{WT}$ and $EGFR^{T790M}$, docking studies were performed, which suggested that most of the synthesized compounds have similar binding modes with a target crystal structure. Therefore, this study presents compounds **11_b** as a potential promising candidate as an EGFR inhibitor.

4. Experimental

4.1. Chemistry

4.1.1. General. All melting points were determined by the open capillary method using a Gallen lamp melting point apparatus. Elemental analyses were performed on a CHN ana-

lyzer. The IR spectra were recorded on a pye Unicam SP 1000 IR spectrophotometer. The progress of reactions was monitored by TLC using TLC sheets coated with UV fluorescent silica gel (Kieselgel 0.25mm, 60 F254, Merck Germany) with a developing solvent system of DCM/methanol (95 : 5) and was visualized using a UV lamp.

NMR spectra were acquired at 600 MHz for ^{1}H and 151 MHz for ^{13}C on either of these two spectrometers: (1) a Bruker Avance NEO-600 equipped with a 1.7 mm TCI CryoProbe, or (2) an Agilent VNMRS-600 equipped with a one-of-a-kind 1.5 mm HTS Cold Probe optimized for 13C detection (see Acknowledgements).[96] Spectra were acquired with these relevant parameters: 1H, 45° pulse, spectral width: 12–16 ppm, acquisition time: 1.1–4.6 s., and relaxation delay: 2–3 s.; 13C and 13C-APT, 45° pulse, spectral width: 240 ppm, acquisition time: 1.0 s., and relaxation delay: 2.0 s. Chemical shifts were expressed in δ (ppm) with reference to TMS and the coupling constant (J) in Hertz using DMSO-d_6 and $CDCl_3$-d_6 as solvents.

Compounds, 4-oxo-6-phenyl-2-thioxo-1,2,3,4-tetrahydropyrimidine-5-carbonitrile **7**,[97–101] 2-(ethylthio)-6-oxo-4-phenyl-1,6-dihydropyrimidine-5-carbonitrile **8$_a$**,[99,102] 2-(butylthio)-6-oxo-4-phenyl-1,6-dihydropyrimidine-5-carbonitrile **8$_b$**,[102] 4-chloro-2-(ethylthio)-6-phenyl-pyrimidine-5-carbonitrile **9$_a$** and 2-(butylthio)-4-chloro-6-phenylpyrimidine-5-carbonitrile **9$_b$**[103] were prepared according to the reported procedures.

4.1.2. General procedure for synthesis of target compounds 10$_{a–h}$–19$_{a,b}$. To a solution of compound **9$_{a,b}$** (0.01 mol) in isopropanol (25 mL) containing a catalytic amount of TEA, the appropriate amine derivatives, namely substituted anilines, 2-aminopyridine, cyclohexylamine, cyclopentylamine, 4-aminoacetophenone, 3-aminoacetophenone, 4-amino-*N*-(4,6-dimethylpyrimidin-2-yl)benzenesulfonamide, benzylamine, phenylhydrazine and/or 4-(2-aminoethyl)benzenesulfonamide (0.01 mol) were added. The reaction mixture was refluxed for 3–6 h. Then, the mixture was concentrated, cooled and poured onto ice/water containing dil. HCl. The formed precipitate was filtered, washed with water and crystallized from ethanol to afford the corresponding target compounds **10$_{a–h}$–19$_{a,b}$**.

*4.1.2.1. 2-(Ethylthio)-4-phenyl-6-(phenylamino)pyrimidine-5-carbonitrile **10$_a$**.* White crystals (yield 72%); mp: 193–194 °C; IR (KBr) ν cm^{-1}: 3298 (NH), 3056 (CH aromatic), 2986, 2924 (CH aliphatic), 2210 (C≡N), 1604 (C=N); ^{1}H NMR (DMSO-d_6) δ ppm; 1.22 (t, 3H, J = 7.2 Hz, –$CH_2C\underline{\mathbf{H}}_3$), 2.98 (q, 2H, J = 7.2 Hz, –$C\underline{\mathbf{H}}_2CH_3$), 7.20 (dd, 1H, J = 7.2 Hz, Ar–H, H-4 of –NHC_6H_5), 7.38 (dd, 2H, J = 7.2 Hz, 7.8 Hz, Ar–H, H-3 & H-5 of –NHC_6H_5), 7.54–7.61 (m, 5H, Ar–H, H-3, H-4 & H-5 of C_6H_5 and H-2 & H-6 of –NHC_6H_5), 7.84 (d, 2H, J = 7.2 Hz, Ar–H, H-2 & H-6 of C_6H_5), 9.82 (s, 1H, exchangeable with D_2O, –NH); ^{13}C NMR (DMSO-d_6) δ (ppm); 14.72, 24.87, 84.62, 116.16, 124.01 (2C), 125.15, 128.47 (2C), 128.67 (2C), 128.76 (2C), 131.27, 136.02, 137.72, 160.33, 168.26, 173.76: APT (DMSO-d_6) δ (ppm); 14.71 (CH_3), 24.87 (CH_2), 84.62 (C), 116.15 (C), 124.01 (2CH), 125.15 (CH), 128.47 (2CH), 128.66 (2CH), 128.75 (2CH), 131.27 (CH), 136.02 (C), 137.71 (C), 160.33 (C), 168.26 (C), 173.75 (C): Anal. Calcd for $C_{19}H_{16}N_4S$ (332.43): C, 68.65; H, 4.85; N, 16.85; found: C, 68.33; H, 5.03; N, 17.00%.

*4.1.2.2. 2-(Butylthio)-4-phenyl-6-(phenylamino)pyrimidine-5-carbonitrile **10$_b$**.* White crystals (yield 78%); mp: 172–173 °C; IR (KBr) ν cm^{-1}: 3290 (NH), 3066 (CH aromatic), 2968, 2931 (CH aliphatic), 2214 (C≡N), 1608 (C=N); ^{1}H NMR (DMSO-d_6) δ ppm; 0.81 (t, 3H, J = 7.2 Hz, –$CH_2CH_2CH_2C\underline{\mathbf{H}}_3$), 1.27 (m, 2H, –$CH_2CH_2C\underline{\mathbf{H}}_2CH_3$), 1.54 (p, 2H, –$CH_2C\underline{\mathbf{H}}_2CH_2CH_3$), 2.97 (t, 2H, J = 7.2 Hz, –$C\mathbf{H}_2CH_2CH_2CH_3$), 7.19 (dd, 1H, J = 7.2 Hz, Ar–H, H-4 of –NHC_6H_5), 7.39 (dd, 2H, J = 7.8 Hz, 9.0 Hz, Ar–H, H-3 & H-5 of –NHC_6H_5), 7.54–7.60 (m, 5H, Ar–H, H-3, H-4 & H-5 of C_6H_5 and H-2 & H-6 of –NHC_6H_5), 7.86 (d, 2H, J = 7.8 Hz, Ar–H, H-2 & H-6 of C_6H_5), 9.82 (s, 1H, exchangeable with D_2O, –NH); ^{13}C NMR (DMSO-d_6) δ (ppm); 13.59, 21.66, 30.03, 31.51, 84.81, 116.03, 124.92 (2C), 125.16, 128.32 (2C), 128.50, 128.62 (2C), 130.74, 135.73, 135.90, 137.63, 160.38, 167.91, 173.64; APT (DMSO-d_6) δ (ppm); 13.35 (CH_3), 21.96 (CH_2), 30.02 (CH_2), 31.50 (CH_2), 84.81 (C), 116.03 (C), 124.00 (2CH), 125.23 (CH), 128.23 (2CH), 128.50 (2CH), 128.62 (2CH), 130.97 (CH) 135.85 (C), 137.87 (C), 160.37 (C), 168.44 (C), 173.63 (C): Anal. Calcd for $C_{21}H_{20}N_4S$ (360.48): 69.97; H, 5.59; N, 15.54. Found: C, 69.53; H, 5.34; N, 15.82%.

*4.1.2.3. 2-(Ethylthio)-4-phenyl-6-(o-tolylamino)pyrimidine-5-carbonitrile **10$_c$**.* White crystals (yield 76%); mp: 142–143 °C; ^{1}H NMR (DMSO-d_6) δ ppm; 1.08 (t, 3H, J = 7.2 Hz, –$CH_2C\underline{\mathbf{H}}_3$), 2.19 (s, 3H, –$C\underline{\mathbf{H}}_3$), 2.83 (q, 2H, J = 7.2 Hz, –$C\underline{\mathbf{H}}_2CH_3$), 7.22–7.24 (m, 2H, Ar–H, H-4 & H-6 of –C_6H_4), 7.29–7.30 (m, 2H, Ar–H, H-3 & H-5 of –C_6H_4), 7.55–7.59 (m, 3H, Ar–H, H-3, H-4 & H-5 of C_6H_5), 7.87 (d, 2H, J = 7.2 Hz, Ar–H, H-2 & H-6 of C_6H_5), 9.58 (s, 1H, exchangeable with D_2O, –NH); ^{13}C NMR (DMSO-d_6) δ (ppm); 14.41, 17.75, 24.69, 83.54, 115.97, 126.07, 126.78, 127.61, 128.46 (2C), 128.55 (2C), 130.22, 131.01, 134.80, 135.94, 136.11, 160.49, 167.81, 173.55: APT (DMSO-d_6) δ (ppm); 14.41 (CH_3), 17.74 (CH_3), 24.69 (CH_2), 83.54 (C), 115.97 (C), 126.07 (CH), 126.87 (CH), 127.61 (CH), 128.46 (2CH), 128.55 (2CH), 130.22 (CH), 131.01 (CH), 134.80 (C), 135.94 (C), 136.11(C), 160.94 (C), 167.81 (C), 173.55 (C): Anal. Calcd for $C_{20}H_{18}N_4S$ (346.45): C, 69.34; H, 5.24; N, 16.17; found: C, 69.54; H, 5.04; N, 16.33, %.

*4.1.2.4. 2-(Butylthio)-4-phenyl-6-(o-tolylamino)pyrimidine-5-carbonitrile (**10$_d$**).* Yellowish white crystals (yield 80%); mp: 127–129 °C; ^{1}H NMR (DMSO-d_6) δ ppm; 0.76 (t, 3H, J = 7.2 Hz, –$CH_2CH_2CH_2C\underline{\mathbf{H}}_3$), 1.13 (m, 2H, –$CH_2CH_2C\underline{\mathbf{H}}_2CH_3$), 1.41 (p, 2H, –$CH_2C\underline{\mathbf{H}}_2CH_2CH_3$), 2.19 (s, 3H, –$CH_3$), 2.77 (t, 2H, J = 7.2 Hz, –$C\mathbf{H}_2CH_2CH_2CH_3$), 7.22–7.24 (m, 2H, Ar–H, H-4 & H-6 of –C_6H_4), 7.27–7.31 (m, 2H, Ar–H, H-3 & H-5 of –C_6H_4), 7.55–7.59 (m, 3H, Ar–H, H-3, H-4 & H-5 of C_6H_5), 7.86 (d, 2H, J = 7.2 Hz, Ar–H, H-2 & H-6 of C_6H_5), 9.64 (s, 1H, exchangeable with D_2O, –NH); ^{13}C NMR (DMSO-d_6) δ (ppm); 13.36, 17.93, 21.42, 29.74, 31.50, 83.72, 116.00, 126.14, 126.91, 127.70, 128.48 (2C), 128.59 (2C), 130.24 131.07, 134.95, 135.95, 136.17, 160.99, 167.90, 173.96; APT (DMSO-d_6) δ (ppm); 13.35 (CH_3), 17.93 (CH_3), 21.37 (CH_2), 29.73 (CH_2), 31.53 (CH_2), 83.10 (C), 116.54 (C), 126.15 (CH), 126.91 (CH), 127.70 (CH), 128.48 (2CH), 128.59 (2CH), 130.24 (CH), 131.04 (CH), 134.94 (C), 135.93 (C), 136.17 (C), 161.31 (C), 167.59 (C), 173.96 (C): Anal. Calcd for $C_{22}H_{22}N_4S$ (374.51): C, 70.56; H, 5.92; N, 14.96; found: C, 70.88; H, 6.15; N, 14.79%.

4.1.2.5. 2-(Ethylthio)-4-phenyl-6-(m-tolylamino)pyrimidine-5-carbonitrile ***10e***. Yellow crystals (yield 70%); mp: 134–135 °C; IR (KBr) ν cm^{-1}: 3294 (NH), 3066, 3039 (CH aromatic), 2966, 2927 (CH aliphatic), 2214 (C≡N), 1620 (C═N); ^{1}H NMR (DMSO-d_6) δ ppm; 1.23 (t, 3H, J = 7.2 Hz, –$CH_2C\underline{H}_3$), 2.30 (s, 3H, –$C\underline{H}_3$), 2.99 (q, 2H, J = 7.2 Hz, –$C\underline{H}_2CH_3$), 7.00 (d, 1H, J = 6.60 Hz, Ar–H, H-4 of –NHC_6H_4), 7.25 (dd, 1H, J = 7.2 Hz, 7.8 Hz, Ar–H, H-5 of –C_6H_4), 7.35 (dd, 1H, J = 7.2 Hz, 7.8 Hz, Ar–H, H-4 of –C_6H_5), 7.42 (s, 1H, Ar–H, H-2 of –NHC_6H_4), 7.55–7.59 (m, 3H, Ar–H, H-3 & H-5 of –C_6H_5 and H-6 of –NHC_6H_4), 7.85 (d, 2H, J = 6.60 Hz, Ar–H, H-2 & H-6 of –C_6H_5), 9.74 (s, 1H, exchangeable with D_2O, –NH); ^{13}C NMR (DMSO-d_6) δ (ppm); 14.68, 21.06, 24.78, 84.50, 116.07, 120.86, 124.34, 125.67, 128.21, 128.56 (2C), 128.68 (2C), 131.16, 135.95, 137.60 (2C), 160.21, 168.14, 173.69; APT (DMSO-d_6) δ (ppm); 14.69 (CH_3), 21.07 (CH_3), 24.79 (CH_2), 84.50 (C), 116.07 (C), 120.86 (CH), 124.34 (CH), 125.67 (CH), 128.21 (CH), 128.56 (2CH), 128.68 (2CH), 131.16 (CH), 135.95 (C), 137.60 (2C), 160.21 (C), 168.14 (C), 173.69 (C): Anal. Calcd for $C_{20}H_{18}N_4S$ (346.45): C, 69.34; H, 5.24; N, 16.17; found C, 69.54; H, 5.12; N, 16.32, %.

4.1.2.6. 2-(Butylthio)-4-phenyl-6-(m-tolylamino)pyrimidine-5-carbonitrile ***10f***. White crystals (yield 82%); mp: 117–118 °C; IR (KBr) ν cm^{-1}: 3302 (NH), 3051 (CH aromatic), 2962, 2927 (CH aliphatic), 2218 (C≡N), 1616 (C═N); ^{1}H NMR (DMSO-d_6) δ ppm; 0.80 (t, 3H, J = 7.2 Hz, –$CH_2CH_2CH_2C\underline{H}_3$), 1.29 (m, 2H, –$CH_2CH_2C\underline{H}_2CH_3$), 1.53 (p, 2H, –$CH_2C\underline{H}_2CH_2CH_3$), 2.31 (s, 3H, –$CH_3$), 2.98 (t, 2H, J = 7.2 Hz, –$C\underline{H}_2CH_2CH_2CH_3$), 7.01 (d, 1H, J = 7.2 Hz, Ar–H, H-4 of –C_6H_4), 7.26 (dd, 1H, J = 7.2 Hz, 7.8 Hz, Ar–H, H-5 of –C_6H_4), 7.35 (dd, 1H, J = 8.4 Hz, 7.8 Hz, Ar–H, H-4 of –C_6H_5), 7.38 (s, 1H, Ar–H, H-2 of –C_6H_4), 7.55–7.59 (m, 3H, Ar–H, H-3 & H-5 of C_6H_5 and H-6 of –C_6H_4), 7.85 (d, 2H, J = 7.8 Hz, Ar–H, H-2 & H-6 of C_6H_5), 9.74 (s, 1H, exchangeable with D_2O, –NH); ^{13}C NMR (DMSO-d_6) δ (ppm); 13.28, 21.17, 21.28, 29.98, 30.98, 84.59, 116.01, 121.12, 124.51, 125.66, 128.14, 128.48 (2C), 128.61 (2C), 131.22, 135.86, 137.53, 137.65, 160.35, 168.12, 173.75; APT (DMSO-d_6) δ (ppm); 13.41 (CH_3), 21.10 (CH_2), 21.26 (CH_3), 30.65 (CH_2), 30.89 (CH_2), 84.50 (C), 116.55 (C), 121.02 (CH), 124.61 (CH), 125.66 (CH), 128.14 (CH), 128.48 (2CH), 128.61 (2CH), 131.19 (CH), 135.89 (C), 137.53 (C), 137.65 (C), 160.29 (C), 168.15 (C), 173.64 (C): Anal. Calcd for $C_{22}H_{22}N_4S$ (374.51): C, 70.56; H, 5.92; N, 14.96; found: C, 70.78; H, 5.81; N, 14.68, %.

*4.1.2.7. 2-(Ethylthio)-4-[(4-methoxyphenyl)amino]-6-phenylpyrimidine-5-carbonitrile (****10g****).* Yellow crystals (yield 82%); mp: 150–151 °C; IR (KBr) ν cm^{-1}: 3298 (NH), 3066, 3039 (CH aromatic), 2968, 2931 (CH aliphatic), 2214 (C≡N), 1604 (C═N); ^{1}H NMR (DMSO-d_6) δ ppm; 1.20 (t, 3H, J = 7.2 Hz, –$CH_2C\underline{H}_3$), 2.96 (q, 2H, J = 7.2 Hz, –$C\underline{H}_2CH_3$), 3.76 (s, 3H, $OC\underline{H}_3$), 6.93 (d, 2H, J = 9.0 Hz, Ar–H, H-3 & H-5 of –C_6H_4), 7.42 (d, 2H, J = 9.0 Hz, Ar–H, H-2 & H-6 of –C_6H_4), 7.53–7.59 (m, 3H, Ar–H, H-3, H-4 & H-5 of –C_6H_5), 7.83 (d, 2H, J = 7.2 Hz, Ar–H, H-2 & H-6 of –C_6H_5), 9.68 (s, 1H, exchangeable with D_2O, –NH); ^{13}C NMR (DMSO-d_6) δ (ppm); 14.75, 24.82, 55.19, 83.73, 113.50 (2C), 116.07, 125.72 (2C), 128.48 (2C), 128.59 (2C), 130.34, 131.03, 136.09, 156.70, 160.40, 167.94, 173.33; APT (DMSO-d_6) δ (ppm); 14.44 (CH_3), 24.83 (CH_2), 55.40 (CH_3), 83.96 (C), 113.50 (2CH), 116.11 (C), 125.72 (2CH), 128.53 (2CH), 128.59 (2CH), 130.34 (C), 130.97 (CH), 135.85 (C), 156.65 (C), 160.14 (C), 167.90 (C), 173.40 (C): Anal. Calcd for $C_{20}H_{18}N_4OS$ (362.45): C, 66.28; H, 5.01; N, 15.46; found: C, 66.51; H, 5.20; N, 15.29, %.

*4.1.2.8. 2-(Butylthio)-4-[(4-methoxyphenyl)amino]-6-phenylpyrimidine-5-carbonitrile (****10h****).* White crystals (yield 85%); mp: 159–160 °C; IR (KBr) ν cm^{-1}: 3294 (NH), 3066 (CH aromatic), 2964, 2931 (CH aliphatic), 2214 (C≡N), 1612 (C═N); ^{1}H NMR (DMSO-d_6) δ ppm; 0.81 (t, 3H, J = 7.2 Hz, –$CH_2CH_2CH_2C\underline{H}_3$), 1.26 (m, 2H, –$CH_2CH_2C\underline{H}_2CH_3$), 1.53 (p, 2H, –$CH_2C\underline{H}_2CH_2CH_3$), 2.94 (t, 2H, J = 7.2 Hz, –$C\underline{H}_2CH_2CH_2CH_3$), 3.76 (s, 3H, –$OCH_3$), 6.94 (d, 2H, J = 8.4 Hz, Ar–H, H-3 & H-5 of –C_6H_4), 7.42 (d, 2H, J = 8.4 Hz, Ar–H, H-2 & H-6 of –C_6H_4), 7.54–7.59 (m, 3H, Ar–H, H-3, H-4 & H-5 of C_6H_5), 7.85 (d, 2H, J = 7.8 Hz, Ar–H, H-2 & H-6 of C_6H_5), 9.65 (s, 1H, exchangeable with D_2O, –NH); ^{13}C NMR (DMSO-d_6) δ (ppm); 13.33, 21.38, 29.92, 31.18, 55.20, 83.86, 113.52 (2C), 116.00, 125.88 (2C), 128.41 (2C), 128.51 (2C), 130.31, 130.97, 135.93, 156.78, 160.40, 167.82, 173.60; APT (DMSO-d_6) δ (ppm); 13.33 (CH_3), 21.50 (CH_2), 29.92 (CH_2), 31.18 (CH_2), 55.20 (CH_3), 83.86 (C), 113.52 (2CH), 116.00 (C), 125.88 (2CH), 128.41 (2CH), 128.51 (2CH), 130.31 (C), 130.97 (CH), 135.93 (C), 156.78 (C), 160.40 (C), 167.82 (C), 173.60 (C): Anal. Calcd for $C_{22}H_{22}N_4OS$ (390.51): C, 67.67; H, 5.68; N, 14.35; found: C, 67.49; H, 5.91; N, 14.08%.

*4.1.2.9. 2-(Ethylthio)-4-phenyl-6-(pyridin-2-ylamino)pyrimidine-5-carbonitrile (****11a****).* Yellowish white crystals (yield 88%); mp: 235–236 °C; ^{1}H NMR (DMSO-d_6) δ ppm; 1.23 (t, 3H, J = 7.2 Hz, –$CH_2C\underline{H}_3$), 2.94 (q, 2H, J = 7.2 Hz, –$C\underline{H}_2CH_3$), 7.10 (dd, 1H, J = 7.2 Hz, 6.6 Hz Ar–H, H-5 of pyridine), 7.25 (d, 1H, J = 9.0 Hz, Ar–H, H-3 of pyridine), 7.44 (dd, 1H, J = 7.2, 7.8 Hz, Ar–H, H-4 of –C_6H_5), 7.53–7.59 (m, 3H, Ar–H, H-4 of pyridine & H-3, H-5 of –C_6H_5), 7.71 (d, 2H, J = 7.8 Hz, Ar–H, H-2 & H-6 of –C_6H_5), 7.80 (d, 1H, J = 7.8 Hz, Ar–H, H-6 of pyridine), 9.21 (s, 1H, exchangeable with D_2O, –NH); ^{13}C NMR (DMSO-d_6) δ (ppm); 14.34, 25.35, 83.09, 103.80, 113.72, 116.38, 127.93 (2C), 128.45 (2C), 129.21, 135.73, 137.08, 150.60, 153.25, 167.35, 172.49, 173.35; APT (DMSO-d_6) δ (ppm); 14.34 (CH_3), 25.35 (CH_2), 83.42 (C), 103.80 (CH), 113.72 (C), 116.83 (CH), 127.93 (2CH), 128.45 (2CH), 129.21 (CH), 135.79 (C), 137.08 (CH), 150.60 (CH), 153.29 (C), 167.35 (C), 172.49 (C), 173.35 (C): Anal. Calcd for $C_{18}H_{15}N_5S$ (333.41): C, 64.84; H, 4.53; N, 21.01; found: C, 64.62; H, 4.23; N, 20.80%.

*4.1.2.10. 2-(Butylthio)-4-phenyl-6-(pyridin-2-ylamino)pyrimidine-5-carbonitrile (****11b****).* Orange crystals (yield 91%); mp: 103–105 °C; 0.81 (t, 3H, J = 7.2 Hz, –$CH_2CH_2CH_2C\underline{H}_3$), 1.31 (m, 2H, –$CH_2CH_2C\underline{H}_2CH_3$), 1.54 (p, 2H, –$CH_2C\underline{H}_2CH_2CH_3$), 2.90 (t, 2H, J = 7.2 Hz, –$C\underline{H}_2CH_2CH_2CH_3$), 7.11 (dd, 1H, J = 7.2 Hz, 6.6 Hz Ar–H, H-5 of pyridine), 7.27 (d, 1H, J = 9.0 Hz, Ar–H, H-3 of pyridine), 7.44 (dd, 1H, J = 7.2 & 7.8 Hz, Ar–H, H-4 of C_6H_5), 7.53–7.57 (m, 3H, H-3, H-5 of C_6H_5 & H-4 of pyridine), 7.78 (d, 2H, J = 7.2 Hz, Ar–H, H-2 & H-6 of C_6H_5), 7.88 (d, 1H, J = 7.8 Hz, Ar–H, H-6 of pyridine), 9.19 (s, 1H, exchangeable with D_2O, –NH); ^{13}C NMR (DMSO-d_6) δ (ppm); 13.40, 21.46, 30.07, 31.07, 85.47, 115.87, 122.54, 128.55 (2C), 128.69 (2C), 128.73

(2C), 131.26, 132.77, 135.74, 142.37, 160.05, 168.24, 173.87; APT (DMSO-d_6) δ (ppm); 13.39 (CH_3), 21.46 (CH_2), 30.07 (CH_2), 31.07 (CH_2), 85.47 (C), 115.87 (C), 122.54 (CH), 128.55 (2CH), 128.69 (2CH), 128.73 (2CH), 131.27 (CH), 132.77 (C), 135.74 (CH), 142.37 (C), 160.05 (C), 168.24 (C), 173.87 (C): Anal. Calcd for $C_{20}H_{19}N_5S$ (361.47): C, 66.46; H, 5.30; N, 19.38; found: C, 66.70; H, 5.12; N, 19.66%.

*4.1.2.11. 4-(Cyclohexylamino)-2-(ethylthio)-6-phenylpyrimidine-5-carbonitrile (**12$_a$**).* Yellow crystals (yield 76%); mp: 200–201 °C; ^{1}H NMR (CDCl$_3$-d_6) δ ppm: 1.27 (m, 2H, CH_2 of cyclohexyl), 1.41 (m, 2H, CH_2 of cyclohexyl), 1.44 (t, 3H, J = 7.2 Hz, –$CH_2C\underline{\mathbf{H}}_3$), 1.68 (m, 2H, CH_2 of cyclohexyl), 1.81 (m, 2H, CH_2 of cyclohexyl), 2.06 (m, 2H, CH_2 of cyclohexyl), 3.15 (q, 2H, J = 7.2 Hz, –$C\underline{\mathbf{H}}_2CH_3$), 4.11 (m, 1H, H-1 of cyclohexyl), 5.57 (br s, 1H, exchangeable with D_2O, –NH), 7.47–7.52 (m, 3H, H-3, H-4, H-5 of C_6H_5), 7.94 (d, 2H, J = 6.6 Hz, Ar–H, H-2 & H-6 of C_6H_5); ^{13}C NMR (CDCl$_3$-d_6) δ (ppm); 14.70, 24.90 (2C), 25.53, 25.76, 32.62 (2C), 50.58, 83.33, 116.85, 128.68 (2C), 128.74 (2C), 131.55, 136.21, 160.92, 166.99, 175.15; APT (CDCl$_3$-d_6) δ (ppm); 14.75 (CH_3), 24.90 ($2CH_2$), 25.53 (CH_2), 25.72 (CH_2), 32.86 ($2CH_2$), 50.58 (CH), 83.37 (C), 116.85 (C), 128.68 (2CH), 128.74 (2CH), 131.34 (CH), 135.88 (C), 160.89 (C), 166.79 (C), 174.89 (C): Anal. Calcd for $C_{19}H_{22}N_4S$ (338.47): C, 67.42; H, 6.55; N, 16.55; found: C, 67.71; H, 6.32; N, 16.80, %.

*4.1.2.12. 2-(Butylthio)-4-(cyclohexylamino)-6-phenylpyrimidine-5-carbonitrile (**12$_b$**).* Orange crystals (yield 77%); mp: 167–168 °C; IR (KBr) ν cm^{-1}: 3309 (NH), 3068 (CH aromatic), 2931 (CH aliphatic), 2214 (C≡N), 1583 (C=N); ^{1}H NMR (CDCl$_3$-d_6) δ ppm; 0.95 (t, 3H, J = 7.2 Hz, –$CH_2CH_2CH_2C\underline{\mathbf{H}}_3$), 1.25 (m, 2H, CH_2 of cyclohexyl), 128 (m, 2H, CH_2 of cyclohexyl), 1.40 (m, 2H, –$CH_2CH_2C\underline{\mathbf{H}}_2CH_3$), 1.49 (m, 2H, CH_2 of cyclohexyl), 1.68 (p, 2H, –$CH_2C\underline{\mathbf{H}}_2CH_2CH_3$), 1.81 (m, 2H, CH_2 of cyclohexyl), 2.06 (m, 2H, CH_2 of cyclohexyl), 3.13 (t, 2H, J = 7.8 Hz, –$C\mathbf{H}_2CH_2CH_2CH_3$), 4.11 (m, 1H, H-1 of cyclohexyl), 5.55 (br s, 1H, exchangeable with D_2O, –NH), 7.46–7.52 (m, 3H, Ar–H, H-3, H-4 & H-5 of $-C_6H_5$), 7.94 (d, 2H, J = 7.8 Hz, Ar–H, H-2 & H-6 of $-C_6H_5$); ^{13}C NMR (CDCl$_3$-d_6) δ (ppm); 13.82, 22.32, 24.94 (2C), 25.67, 31.05, 31.79 (2C), 32.89, 50.53, 83.25, 116.91, 128.66 (2C), 128.73 (2C), 131.30, 135.87, 160.95, 166.82, 175.08; APT (CDCl$_3$-d_6) δ (ppm); 13.81 (CH_3), 22.32 (CH_2), 24.94 ($2CH_2$), 25.53 (CH_2), 31.05 (CH_2), 31.79 ($2CH_2$), 32.89 (CH_2), 50.53 (CH), 83.25 (C), 116.91 (C), 128.66 (2CH), 128.73 (2CH), 131.29 (CH), 135.87 (C), 160.95 (C), 166.82 (C), 175.09 (C): Anal. Calcd for $C_{21}H_{26}N_4S$ (366.53): C, 68.82; H, 7.15; N, 15.29; found: C, 69.03; H, 6.93; N, 15.45%.

*4.1.2.13. 4-(Cyclopentylamino)-2-(ethylthio)-6-phenylpyrimidine-5-carbonitrile **13$_a$**.* Yellow crystals (yield 69%); mp: 135–137 °C; ^{1}H NMR (CDCl$_3$-d_6) δ ppm: 1.42 (t, 3H, J = 7.2 Hz, –$CH_2C\underline{\mathbf{H}}_3$), 1.55 (m, 2H, CH_2 of cyclopentyl), 1.68 (m, 2H, CH_2 of cyclopentyl), 1.77 (m, 2H, CH_2 of cyclopentyl), 2.12 (m, 2H, CH_2 of cyclohexyl), 3.17 (q, 2H, J = 7.2 Hz, –$C\underline{\mathbf{H}}_2CH_3$), 4.51 (m, 1H, H-1 of cyclopentyl), 5.63 (br s, 1H, exchangeable with D_2O, –NH), 7.47–7.51 (m, 3H, H-3, H-4, H-5 of phenyl), 7.94 (d, 2H, J = 6.6 Hz, Ar–H, H-2 & H-6 of phenyl); ^{13}C NMR (CDCl$_3$-d_6) δ (ppm); 14.70, 23.98 (2C), 25.70, 33.30 (2C), 53.42, 83.38, 116.89, 128.74 (4C), 131.34, 135.79, 161.31, 166.69, 175.12; APT (CDCl$_3$-d_6) δ (ppm); 14.76 (CH_3), 23.98 ($2CH_2$), 25.86 (CH_2), 33.33 ($2CH_2$), 53.42 (CH), 83.46 (C), 116.89 (C), 128.74 (4CH), 131.06 (CH), 135.80 (C), 161.05 (C), 166.69 (C), 174.83 (C): Anal. Calcd for $C_{18}H_{20}N_4S$ (324.45): C, 66.64; H, 6.21; N, 17.27; found: C, 66.43; H, 6.45; N, 17.03, %.

*4.1.2.14. 2-(Butylthio)-4-(cyclopentylamino)-6-phenylpyrimidine-5-carbonitrile **13$_b$**.* Yellowish white crystals (yield 75%); mp: 139–140 °C; ^{1}H NMR (DMSO-d_6) δ ppm; 0.91 (t, 3H, J = 7.8 Hz, –$CH_2CH_2CH_2C\underline{\mathbf{H}}_3$), 1.41 (m, 2H, –$CH_2CH_2C\underline{\mathbf{H}}_2CH_3$), 1.54 (m, 2H, –$CH_2C\underline{\mathbf{H}}_2CH_2CH_3$), 166–1.72 (m, 6H, 3($CH_2$) of cyclopentyl), 1.94 (m, 2H, CH_2 of cyclopentyl), 3.09 (t, 2H, J = 7.8 Hz, –$C\mathbf{H}_2CH_2CH_2CH_3$), 4.46 (m, 1H, H-1 of cyclopentyl), 7.51–7.57 (m, 3H, Ar–H, H-3, H-4 & H-5 of $-C_6H_5$), 7.76 (br s, 1H, exchangeable with D_2O, –NH), 7.80 (d, 2H, J = 7.2 Hz, Ar–H, H-2 & H-6 of $-C_6H_5$); ^{13}C NMR (DMSO-d_6) δ (ppm); 13.36, 21.92, 23.55 (2C), 30.00, 31.29, 31.77 (2C), 53.11, 83.06, 116.19, 128.34 (2C), 128.41 (2C), 130.81, 136.00, 160.95, 167.32, 173.35; APT (DMSO-d_6) δ (ppm); 13.44 (CH_3), 21.58 (CH_2), 23.60 ($2CH_2$), 30.04 (CH_2), 31.34 (CH_2), 31.62 ($2CH_2$), 52.81 (CH), 83.17 (C), 116.26 (C), 128.40 (2CH), 128.47 (2CH), 130.87 (CH), 136.08 (C), 160.69 (C), 167.18 (C), 173.56 (C): Anal. Calcd for $C_{20}H_{24}N_4S$ (352.50): C, 68.15; H, 6.86; N, 15.89; found: C, 68.41; H, 7.05; N, 16.12, %.

*4.1.2.15. 4-[(4-Acetylphenyl) amino]-2-(ethylthio)-6-phenylpyrimidine-5-carbonitrile **14$_a$**.* White crystals (yield 84%); mp: 190–191 °C; IR (KBr) ν cm^{-1}: 3294, (NH), 3066 (CH aromatic), 2974, 2936 (CH aliphatic), 2214 (C≡N), 1681 (C=O), 1600 (C=N); ^{1}H NMR (DMSO-d_6) δ (ppm); 1.29 (t, 3H, J = 7.2 Hz, –$CH_2C\underline{\mathbf{H}}_3$), 2.56 (s, 3H, –$COC\underline{\mathbf{H}}_3$), 3.09 (q, 2H, J = 7.2 Hz, –$C\underline{\mathbf{H}}_2CH_3$), 7.57–7.63 (m, 3H, H-3, H-4, H-5 of $-C_6H_5$), 7.79 (d, 2H, J = 8.4 Hz, Ar–H, H-2 & H-6 of $-C_6H_4$), 7.88 (d, 2H, J = 7.8 Hz, Ar–H, H-2 & H-6 of $-C_6H_5$), 7.98 (d, 2H, J = 8.4 Hz, Ar–H, H-3 & H-5 of $-C_6H_4$), 10.04 (br s, 1H, exchangeable with D_2O, –NH); ^{13}C NMR (DMSO-d_6) δ (ppm); 14.47, 24.82, 26.48, 85.56, 115.77, 122.24 (2C), 128.53 (2C), 128.65 (2C), 128.71 (2C), 131.22, 132.75, 135.74, 142.32, 159.96, 168.28, 173.77, 196.69; APT (DMSO-d_6) δ (ppm); 14.47 (CH_3), 24.81 (CH_2), 26.48 (CH_3), 85.56 (C), 115.77 (C), 122.27 (2CH), 128.53 (2CH), 128.65 (2CH), 128.71 (2CH), 131.22 (CH), 132.75 (C), 135.74 (C), 142.34 (C), 159.96 (C), 168.28 (C), 173.77 (C), 196.69 (C): Anal. Calcd for $C_{21}H_{18}N_4OS$ (374.46): C, 67.36; H, 4.85; N, 14.96; found: C, 67.13; H, 5.09; N, 14.71, %.

*4.1.2.16. 4-[(4-Acetylphenyl) amino]-2-(butylthio)-6-phenylpyrimidine-5-carbonitrile **14$_b$**.* Yellowish white crystals (yield 78%); mp: 180–181 °C; IR (KBr) ν cm^{-1}: 3298, (NH), 3070 (CH aromatic), 2998, 2931 (CH aliphatic), 2214 (C≡N), 1678 (C=O), 1604 (C=N); ^{1}H NMR (DMSO-d_6) δ (ppm); 0.81 (t, 3H, J = 7.2 Hz, –$CH_2CH_2CH_2C\underline{\mathbf{H}}_3$), 1.32 (m, 2H, –$CH_2CH_2C\underline{\mathbf{H}}_2CH_3$), 1.60 (p, 2H, –$CH_2C\underline{\mathbf{H}}_2CH_2CH_3$), 2.56 (s, 3H, –$COC\underline{\mathbf{H}}_3$), 3.04 (t, 2H, J = 7.2 Hz, –$C\mathbf{H}_2CH_2CH_2CH_3$), 7.56–7.61 (m, 3H, H-3, H-4, H-5 of $-C_6H_5$), 7.77 (d, 2H, J = 8.4 Hz, Ar–H, H-2 & H-6 of $-C_6H_4$), 7.87 (d, 2H, J = 7.2 Hz, Ar–H, H-2 & H-6 of $-C_6H_5$), 7.97 (d, 2H, J = 8.4 Hz, Ar–H, H-3 & H-5 of $-C_6H_4$), 10.09 (br s, 1H, exchangeable with D_2O, –NH); ^{13}C NMR (DMSO-d_6) δ (ppm); 13.39, 21.46, 26.52, 30.07, 31.07, 85.47, 115.88, 122.45 (2C),

128.55 (2C), 128.69 (2C), 128.73 (2C), 131.27, 132.77, 135.74, 142.38, 160.05, 168.24, 173.86, 196.66: APT (DMSO-d_6) δ (ppm); 13.39 (CH_3), 21.46 (CH_2), 26.52 (CH_3), 30.07 (CH_2), 31.07 (CH_2), 85.47 (C), 115.87 (C), 122.54 (2CH), 128.55 (2CH), 128.69 (2CH), 128.72 (2CH), 131.27 (CH), 132.77 (C), 135.74 (C), 142.38 (C), 160.05 (C), 168.24 (C), 173.86 (C), 196.66 (C): Anal. Calcd for $C_{23}H_{22}N_4OS$ (402.52): C, 68.63; H, 5.51; N, 13.92; found: C, 68.44; H, 5.84; N, 14.15, %.

*4.1.2.17. 4-[(3-Acetylphenyl) amino]-2-(ethylthio)-6-phenylpyrimidine-5-carbonitrile (**15$_a$**).* Yellow crystals (yield 73%); mp: 183–185 °C; IR (KBr) ν cm^{-1}: 3294, (NH), 3066 (CH aromatic), 2974, 2936 (CH aliphatic), 2214 (C≡N), 1681 (C═O), 1600 (C═N); ^{1}H NMR (CDCl$_3$-d_6) δ ppm; 1.21 (t, 3H, J = 7.2 Hz, $-CH_2C\underline{\mathbf{H}}_3$), 2.59 (s, 3H, $COC\underline{\mathbf{H}}_3$), 3.03 (q, 2H, J = 7.2 Hz, $-C\underline{\mathbf{H}}_2CH_3$), 7.54 (dd, 1H, J = 7.8 Hz, Ar–H, H-5 of $-C_6H_4$), 7.56–7.62 (m, 3H, Ar–H, H-3, H-4 & H-5 of $-C_6H_5$), 7.79 (d, 1H, J = 7.8 Hz, Ar–H, H-4 of $-C_6H_4$), 7.86–7.87 (m, 3H, Ar–H, H-6 of $-C_6H_4$ and H-2 & H-6 of $-C_6H_5$), 8.21 (s, 1H, Ar–H, H-2 of $-C_6H_4$), 10.01 (s, 1H, exchangeable with D_2O, –NH); ^{13}C NMR (CDCl$_3$-d_6) δ (ppm); 14.47, 25.97, 26.91, 84.66, 116.43, 121.76, 125.25, 126.44, 128.89 (2C), 128.91 (2C), 129.37, 131.87, 135.49, 137.74, 138.09, 160.14, 167.51, 175.69, 197.53; APT (CDCl$_3$-d_6) δ (ppm); 14.38 (CH_3), 26.10 (CH_2), 26.98 (CH_3), 84.66 (C), 116.44 (C), 121.70 (CH), 125.25 (CH), 126.44 (CH), 128.89 (2CH), 128.90 (2CH), 129.43 (CH), 131.76 (CH), 135.46 (C), 137.73 (C), 138.13 (C), 160.17 (C), 167.55 (C), 175.70 (C), 197.39 (C): Anal. Calcd for $C_{21}H_{18}N_4OS$ (374.46): C, 67.36; H, 4.85; N, 14.96; found: C, 67.19; H, 4.66; N, 14.79, %.

*4.1.2.18. 4-[(3-Acetylphenyl) amino]-2-(butylthio)-6-phenylpyrimidine-5-carbonitrile (**15$_b$**).* Yellowish white crystals (yield 79%); mp: 154–156 °C; IR (KBr) ν cm^{-1}: 3298, (NH), 3070 (CH aromatic), 2998, 2931 (CH aliphatic), 2214 (C≡N), 1678 (C═O), 1604 (C═N); ^{1}H NMR (DMSO-d_6) δ ppm; 0.77 (t, 3H, J = 7.2 Hz, $-CH_2CH_2CH_2C\underline{\mathbf{H}}_3$), 1.24 (m, 2H, $-CH_2CH_2C\underline{\mathbf{H}}_2CH_3$), 1.52 (p, 2H, $-CH_2C\underline{\mathbf{H}}_2CH_2CH_3$), 2.58 (s, 3H, $-COC\mathbf{H}_3$), 2.99 (t, 2H, J = 7.8 Hz, $-C\mathbf{H}_2CH_2CH_2CH_3$), 7.55 (dd, 1H, J = 7.8 & 8.0 Hz, Ar–H, H-5 of $-C_6H_4$), 7.58–7.60 (m, 3H, Ar–H, H-3, H-4 & H-5 of $-C_6H_5$), 7.79 (d, 1H, J = 7.8 Hz, Ar–H, H-4 of $-C_6H_4$), 7.84 (d, 1H, J = 8.0 Hz, Ar–H, H-6 of $-C_6H_4$), 7.87 (d, 2H, J = 7.8 Hz, Ar–H, H-2 & H-6 of $-C_6H_5$), 8.18 (s, 1H, Ar–H, H-2 of $-C_6H_4$), 9.96 (s, 1H, exchangeable with D_2O, –NH); ^{13}C NMR (DMSO-d_6) δ (ppm); 13.28, 21.29, 26.65, 29.97, 30.84, 84.69, 115.84, 123.33, 124.67, 128.31 (2C), 128.46 (2C), 128.57, 128.64, 131.06, 135.79, 137.09, 138.12, 160.25, 168.02, 173.75, 197.17; APT (DMSO-d_6) δ (ppm); 13.28 (CH_3), 21.29 (CH_2), 26.63 (CH_3), 29.97 (CH_2), 30.86 (CH_2), 84.69 (C), 115.84 (C), 123.33 (CH), 124.66 (CH), 128.30 (2CH), 128.45 (2CH), 128.57 (CH), 128.64 (CH), 131.10 (CH), 135.79 (C), 137.09 (C), 138.12 (C), 160.25 (C), 168.02 (C), 173.75 (C), 197.35 (C): Anal. Calcd for $C_{23}H_{22}N_4OS$ (402.52): C, 68.63; H, 5.51; N, 13.92; found: C, 68.82; H, 5.33; N, 13.65, %.

*4.1.2.19. 4-[(5-Cyano-2-(ethylthio)-6-phenylpyrimidin-4-yl)-amino]-N-(4,6-dimethyl pyrimidin-2-yl)benzenesulfonamide (**16$_a$**).* White crystals (yield 87%); mp: 245–246 °C; IR (KBr) ν cm^{-1}: 3314, 3213 (2 NH), 3093, 3062 (CH aromatic), 2970, 2924 (CH aliphatic), 2218 (C≡N), 1597 (C═N), 1319, 1165 (SO_2); ^{1}H NMR (DMSO-d_6) δ (ppm); 1.17 (t, 3H, J = 7.2 Hz, $-CH_2C\underline{\mathbf{H}}_3$), 2.25 (s, 6H, 2($C\mathbf{H}_3$), 3.01 (q, 2H, J = 7.2 Hz, $-C\underline{\mathbf{H}}_2CH_3$), 6.74 (s, 1H, Ar–H, H-5 of dimethylpyrimidine), 7.55–7.61 (m, 3H, Ar–H, H-3, H-4 & H-5 of $-C_6H_5$), 7.77 (d, 2H, J = 8.4 Hz, Ar–H, H-3 & H-5 of $-C_6H_4$), 7.86 (d, 2H, J = 7.20 Hz, Ar–H, H-2 & H-6 of $-C_6H_5$), 7.98 (d, 2H, J = 8.4 Hz, Ar–H, H-2 & H-6 of $-C_6H_4$), 10.12 (s, 1H, exchangeable with D_2O, –NH); ^{13}C NMR (DMSO-d_6) δ ppm; 14.44, 22.89, 24.87 (2C), 85.50, 111.80, 115.92, 122.45, 128.63 (3C), 128.66 (2C), 128.77, 131.36, 135.81 (2C), 141.70, 156.39, 160.14, 168.39 (2C), 173.83 (2C): Anal. Calcd for $C_{25}H_{23}N_7O_2S_2$ (517.63): C, 58.01; H, 4.48; N, 18.94; found: C, 57.80; H, 4.70; N, 19.13, %.

*4.1.2.20. 4-((2-(Butylthio)-5-cyano-6-phenylpyrimidin-4-yl)-amino)-N-(4,6-dimethyl pyrimidin-2-yl)benzenesulfonamide **16$_b$**.* Light green crystals (yield 79%); mp: 209–210 °C; IR (KBr) ν cm^{-1}: 3314, 3213 (2 NH), 3093, 3062 (CH aromatic), 2970, 2924 (CH aliphatic), 2218 (C≡N), 1597 (C═N), 1319, 1165 (SO_2); ^{1}H NMR (DMSO-d_6) δ ppm; 0.75 (t, 3H, J = 7.2 Hz, $-CH_2CH_2CH_2C\underline{\mathbf{H}}_3$), 1.22 (m, 2H, $-CH_2CH_2C\underline{\mathbf{H}}_2CH_3$), 1.51 (p, 2H, $-CH_2C\underline{\mathbf{H}}_2CH_2CH_3$), 2.26 (s, 6H, 2$C\mathbf{H}_3$), 2.99 (t, 2H, J = 7.2 Hz, $-C\mathbf{H}_2CH_2CH_2CH_3$), 6.76 (s, 1H, Ar–H, H-5 of dimethylpyrimidine), 7.55–7.61 (m, 3H, Ar–H, H-3, H-4 & H-5 of $-C_6H_5$), 7.76 (d, 2H, J = 8.4 Hz, Ar–H, H-3 & H-5 of $-C_6H_4$), 7.86 (d, 2H, J = 7.8 Hz, Ar–H, H-2 & H-6 of $-C_6H_5$), 7.99 (d, 2H, J = 8.4 Hz, Ar–H, H-2 & H-6 of $-C_6H_4$), 10.10 (s, 1H, exchangeable with D_2O, –NH); ^{13}C NMR (DMSO-d_6) δ (ppm); 13.35, 21.34, 24.15 (2C), 30.00, 31.05, 85.14, 111.80, 115.69, 122.61, 128.55 (3C), 128.68 (2C), 128.97, 130.31, 131.27, 135.71 (2C), 141.43, 156.32, 160.18, 168.24 (2C), 173.82 (2C); APT (DMSO-d_6) δ (ppm); 13.35 (CH_3), 21.33 (CH_2), 24.20 (2CH_3), 30.00 (CH_2), 31.05 (CH_2), 85.36 (C), 111.82 (CH), 115.82 (C), 122.49 (CH), 128.55 (3CH), 128.68 (2CH), 128.97 (CH), 130.33 (CH), 131.26 (CH), 135.71 (2C), 141.57 (C), 156.15 (C), 160.10 (C), 168.25 (2C), 173.82 (2C): Anal. Calcd for $C_{27}H_{27}N_7O_2S_2$ (545.68): C, 59.43; H, 4.99; N, 17.97; found: C, 59.21; H, 5.16; N, 17.78, %.

*4.1.2.21. 4-(Benzylamino)-2-(ethylthio)-6-phenylpyrimidine-5-carbonitrile **17$_a$**.* Yellow crystals (yield 79%); mp: 160–161 °C; IR (KBr) ν cm^{-1}: 3329 (NH), 3062 (CH aromatic), 2974, 2927 (CH aliphatic), 2214 (C≡N), 1573 (C═N); ^{1}H NMR (DMSO-d_6) δ ppm; 1.19 (t, 3H, J = 7.2 Hz, $-CH_2C\underline{\mathbf{H}}_3$), 2.99 (q, 2H, J = 7.2 Hz, $-C\underline{\mathbf{H}}_2CH_3$), 4.66 (s, 2H, $-NHC\underline{\mathbf{H}}_2$), 7.24 (dd, 1H, J = 6.0, 6.6 Hz Ar–H, H-4 of benzyl), 7.31–7.34 (m, 4H, Ar–H, of benzyl), 7.52–7.57 (m, 3H, H-3, H-4 & H-5 of phenyl), 7.83 (d, 2H, J = 7.2 Hz, Ar–H, H-2 & H-6 of phenyl), 8.70 (s, 1H, exchangeable with D_2O, –NH); ^{13}C NMR (DMSO-d_6) δ (ppm); 14.75, 24.84, 44.15, 83.09, 116.31, 126.82, 127.10 (2C), 128.28 (2C), 128.46 (2C), 128.48 (2C), 130.96, 136.02, 138.99, 161.18, 167.24, 173.59; APT (DMSO-d_6) δ (ppm); 14.66 (CH_3), 24.69 (CH_2), 44.20 (CH_2), 83.42 (C), 116.01 (CH), 126.82 (CH), 127.09 (2CH), 128.28 (2CH), 128.45 (2CH), 128.48 (2CH), 130.42 (C), 136.04 (C), 139.04 (C), 161.53 (C), 167.36 (C), 173.64 (C): Anal. Calcd for $C_{20}H_{18}N_4S$ (346.45): C, 69.34; H, 5.24; N, 16.17; found: C, 69.21; H, 5.40; N, 16.31, %.

*4.1.2.22. 4-(Benzylamino)-2-(butylthio)-6-phenylpyrimidine-5-carbonitrile **17$_b$**.* Yellow crystals (yield 82%); mp: 124–125 °C; ^{1}H NMR (DMSO-d_6) δ ppm; 0.80 (t, 3H, J = 7.2 Hz,

–$CH_2CH_2CH_2C\underline{H}_3$), 1.29 (m, 2H, –$CH_2CH_2C\underline{H}_2CH_3$), 1.52 (p, 2H, –$CH_2C\underline{H}_2CH_2CH_3$), 2.99 (t, 2H, J = 7.2 Hz, –$CH_2CH_2CH_2CH_3$), 4.67 (s, 2H, –NHCH_2), 7.24 (dd, 1H, J = 8.4, 6.6 Hz Ar–H, H-4 of benzyl), 7.32–7.33 (m, 4H, Ar–H, of benzyl), 7.52–7.58 (m, 3H, H-3, H-4 & H-5 of C_6H_5), 7.83 (d, 2H, J = 7.2 Hz, Ar–H, H-2 & H-6 of C_6H_5), 8.68 (s, 1H, exchangeable with D_2O, –NH); ^{13}C NMR (DMSO-d_6) δ (ppm); 13.39, 21.42, 29.99, 31.07, 44.07, 83.22, 116.24, 126.82, 126.98 (2C), 128.28 (2C), 128.46 (2C), 128.49 (2C), 130.99, 135.94, 138.75, 161.23, 167.09 (C), 173.71 (C); APT (DMSO-d_6) δ (ppm); 13.45 (CH_3), 21.42 (CH_2), 29.99 (CH_2), 31.07 (CH_2), 44.06 (CH_2), 83.17 (C), 116.24 (C), 126.82 (CH), 126.98 (2CH), 128.28 (2CH), 128.46 (2CH), 128.49 (2CH), 130.99 (CH), 135.94 (C), 138.75 (C), 161.23 (C), 167.09 (C), 173.71 (C): Anal. Calcd for $C_{22}H_{22}N_4S$ (374.51): C, 70.56; H, 5.92; N, 14.96; found: C, 70.31; H, 6.14; N, 14.77, %.

4.1.2.23. 2-(Ethylthio)-4-phenyl-6-(2-phenylhydrazinyl)pyrimidine-5-carbonitrile ***18$_a$***. White crystals (yield 83%); mp: 167–168 °C; IR (KBr) ν cm^{-1}: 3363, 3294, 3197, 3163 (NH) &NH_2, 3089 (CH aromatic), 2962, 2924 (CH aliphatic), 2206 (C≡N), 1635, 1600 (C=N); ^{1}H NMR (DMSO-d_6) δ (ppm); 1.41 (t, 3H, J = 7.2 Hz, –$CH_2C\underline{H}_3$), 3.23 (q, 2H, J = 7.2 Hz, –C$\underline{H}_2CH_3$), 6.75 (dd, 1H, J = 7.2, 7.8 Hz, Ar–H, H-4 of C_6H_5NH–), 6.79 (d, 2H, J = 7.2 Hz, Ar–H, H-2 & H-6 of C_6H_5NH–), 7.17 (dd, 2H, J = 7.2, 7.8 Hz, Ar–H, H-3 & H-5 of C_6H_5NH–), 7.51–7.56 (m, 3H, H-3, H-4, H-5 of –C_6H_5), 7.86 (d, 2H, J = 7.6 Hz, Ar–H, H-2 & H-6 of –C_6H_5), 8.17 (br s, 1H, exchangeable with D_2O, –NH), 10.02 (br s, 1H, exchangeable with D_2O, –NH); ^{13}C NMR (DMSO-d_6) δ (ppm); 14.46, 24.63, 81.95, 112.40 (2C), 119.51, 124.93, 128.38, 128.64 (2C), 128.80, 128.88, 128.94, 129.04, 136.08, 148.69, 161.48, 169.22, 173.73; APT (DMSO-d_6) δ (ppm); 14.46 (CH_3), 24.75 (CH_2), 81.83 (C), 112.40 (2CH), 119.51 (C), 124.93 (CH), 128.38 (CH), 128.64 (2CH), 128.80 (CH), 128.88 (CH), 128.94 (CH), 129.03 (CH), 136.12 (C), 148.69 (C), 161.84 (C), 169.22 (C), 173.73 (C): Anal. Calcd for $C_{19}H_{17}N_5S$ (347.44): C, 65.68; H, 4.93; N, 20.16; found: C, 65.45; H, 4.65; N, 19.81%.

4.1.2.24. 2-(Butylthio)-4-phenyl-6-(2-phenylhydrazinyl)pyrimidine-5-carbonitrile ***18$_b$***. Light green crystals (yield 70%); mp: 117–118 °C; IR (KBr) ν cm^{-1}: 3309, 3197, 3170 (NH) &NH_2, 3089 (CH aromatic), 2964, 2931 (CH aliphatic), 2206 (C≡N), 1635, 1600 (C=N); ^{1}H NMR (DMSO-d_6) δ ppm; 0.93 (t, 3H, J = 7.2 Hz, –$CH_2CH_2CH_2C\underline{H}_3$), 1.48 (m, 2H, –$CH_2CH_2C\underline{H}_2CH_3$), 1.76 (p, 2H, –$CH_2C\underline{H}_2CH_2CH_3$), 3.21 (t, 2H, J = 7.2 Hz, –C$\underline{H}_2CH_2CH_2CH_3$), 5.43 (s, 2H, exchangeable with D_2O, 2 –NH), 7.26 (dd, 1H, J = 7.2, 7.8 Hz, Ar–H, H-4 of C_6H_5NH–), 7.51 (d, 2H, J = 7.8 Hz, Ar–H, H-2 & H-6 of C_6H_5NH–), 7.52–7.62 (m, 3H, Ar–H, H-3 & H-5 of C_6H_5NH- and H-4 of C_6H_5), 7.86 (dd, 2H, J = 7.2, 8.4 Hz, H-3 H-5 of & C_6H_5), 8.19 (d, 2H, J = 8.4 Hz, Ar–H, H-2 & H-6 of C_6H_5); ^{13}C NMR (DMSO-d_6) δ (ppm); 13.51, 21.73, 30.21, 31.19, 102.18, 119.74 (2C), 124.95, 128.87 (2C), 129.00 (4C), 130.79, 136.06, 138.63, 148.76, 153.26, 161.83, 169.27; APT (DMSO-d_6) δ (ppm); 13.54 (CH_3), 21.72 (CH_2), 30.20 (CH_2), 31.19 (CH_2), 102.18 (C), 119.74 (2CH), 124.95 (CH), 128.87 (2CH), 129.00 (4CH), 130.79 (CH), 136.05 (C), 138.62 (C), 148.75 (C), 153.26 (C), 161.83 (C), 169.26 (C): Anal. Calcd for $C_{21}H_{21}N_5S$ (375.49): C, 67.17; H, 5.64; N, 18.65; found: C, 67.36; H, 5.36; N, 18.90, %.

4.1.2.25. 4-(2-((5-Cyano-2-(ethylthio)-6-phenylpyrimidin-4-yl)-amino) ethyl) benzene sulfonamide ***19$_a$***. Yellow crystals (yield 75%); mp: 213–215 °C; IR (KBr) ν cm^{-1}: 3362, 3236 (NH & NH_2), 3088, 3051 (CH aromatic), 2978, 2931 (CH aliphatic), 2206 (C≡N), 1593 (C=N), 1300, 1161 (SO_2); ^{1}H NMR (DMSO-d_6) δ ppm; 1.35 (t, 3H, J = 7.2 Hz, –$CH_2C\underline{H}_3$), 2.99 (t, 2H, J = 7.2 Hz, –C$\underline{H}_2CH_2NH$), 3.14 (q, 2H, J = 7.2 Hz, –C$\underline{H}_2CH_3$), 3.71 (t, 2H, J = 7.2 Hz, –$CH_2C\underline{H}_2NH$), 7.30 (s, 2H, exchangeable with D_2O, –NH_2), 7.43 (d, 2H, J = 7.8 Hz, Ar–H, H-3 & H-5 of –C_6H_4), 7.53–7.59 (m, 3H, Ar–H, H-3, H-4 & H-5 of –C_6H_5), 7.78 (d, 2H, J = 7.8 Hz, Ar–H, H-2 & H-6 of –C_6H_4), 7.83 (d, 2H, J = 7.8 Hz, Ar–H, H-2 & H-6 of –C_6H_5), 8.19 (br s, 1H, exchangeable with D_2O, –NH); ^{13}C NMR (DMSO-d_6) δ (ppm); 14.75, 24.84, 34.39, 41.92, 83.11, 116.32, 125.79 (2C), 128.47 (3C), 129.04 (2C), 130.99, 135.90 (2C), 142.25, 143.40, 161.27, 167.05, 173.83; APT (DMSO-d_6) δ (ppm); 14.70 (CH_3), 24.81 (CH_2), 34.35 (CH_2), 42.00 (CH_2), 83.15 (C), 116.20 (C), 125.79 (2CH), 128.47 (3CH), 129.09 (2CH), 130.99 (2CH), 135.95 (C), 142.18 (C) 143.30 (C), 161.16 (C), 167.05 (C), 173.68 (C): Anal. Calcd for $C_{21}H_{21}N_5O_2S_2$ (439.55): C, 57.38; H, 4.82; N, 15.93; found: C, 57.70; H, 5.00; N, 15.67%.

*4.1.2.26. 4-(2-((2-(Butylthio)-5-cyano-6-phenylpyrimidin-4-yl)-amino) ethyl) benzene sulfonamide (***19$_b$***).* Yellowish white crystals (yield 73%); mp: 198–199 °C; 3363, 3271 (NH & NH_2), 3086, 3062 (CH aromatic), 2968, 2931 (CH aliphatic), 2210 (C≡N), 1593 (C=N), 1323, 1157 (SO_2); ^{1}H NMR (DMSO-d_6) δ ppm; 0.88 (t, 3H, J = 7.8 Hz, –$CH_2CH_2CH_2C\underline{H}_3$), 1.41 (m, 2H, –$CH_2CH_2C\underline{H}_2CH_3$), 1.68 (p, 2H, –$CH_2C\underline{H}_2CH_2CH_3$), 2.99 (t, 2H, J = 7.2 Hz, –C$\underline{H}_2CH_2NH$), 3.13 (t, 2H, J = 7.2 Hz, –C$H_2CH_2CH_2CH_3$), 3.72 (t, 2H, J = 7.2 Hz, –$CH_2C\underline{H}_2NH$), 7.27 (s, 2H, exchangeable with D_2O, –NH_2), 7.43 (d, 2H, J = 7.8 Hz, Ar–H, H-3 & H-5 of –C_6H_4), 7.52–7.58 (m, 3H, Ar–H, H-3, H-4 & H-5 of –C_6H_5), 7.78 (d, 2H, J = 7.2 Hz, Ar–H, H-2 & H-6 of –C_6H_4), 7.83 (d, 2H, J = 7.8 Hz, Ar–H, H-2 & H-6 of –C_6H_5), 8.13 (br s, 1H, exchangeable with D_2O, –NH); ^{13}C NMR (DMSO-d_6) δ (ppm); 13.42, 21.45, 30.03, 31.07, 34.25, 41.87, 83.10, 116.12, 125.70 (2C), 128.39 (4C), 128.99 (2C), 130.93, 135.90, 142.18, 143.23, 161.13, 166.94, 173.74; APT (DMSO-d_6) δ (ppm); 13.42 (CH_3), 21.45 (CH_2), 30.03 (CH_2), 31.01 (CH_2), 34.25 (CH_2), 41.88 (CH_2), 83.10 (C), 116.12 (C), 125.70 (2CH), 128.39 (4CH), 128.99 (2CH), 130.92 (CH), 135.90 (C), 142.18 (C) 143.23 (C), 161.13 (C), 166.94 (C), 173.74 (C): Anal. Calcd for $C_{23}H_{25}N_5O_2S_2$ (467.61): C, 59.08; H, 5.39; N, 14.98; found: C, 58.79; H, 5.68; N, 15.17%.

4.2. Biological evaluation

4.2.1. *In vitro* antiproliferative activities. The *in vitro* antiproliferative activities of all the synthesized compounds against a panel of four human tumor cell lines, namely colorectal carcinoma (HCT-116), hepatocellular carcinoma (HepG-2), breast cancer (MCF-7) and non-small cell lung cancer cells (A549), were evaluated quantitatively as described in the literature, using the MTT assay protocol.[75–77,104,105] Two

commercially available drugs (doxorubicin and erlotinib) were used in this test as positive controls. The anti-proliferative activity was assessed quantitatively as follows.

Human cancer cell lines were dropped in 96-well plates at a density of 3–8 × 10^3 cells per well. Next, the wells were incubated for 12 h in a 5% CO_2 incubator at 37 °C. Then, for each well, the growth medium was exchanged with 0.1 ml of fresh medium containing graded concentrations of the test compounds to reach the concentration of DMSO. The wells were incubated for two days. Then 10 μl MTT solution (5 μg ml^{-1}) was added into each well, and the cells were incubated for an additional 4 h. The crystals of MTT-formazan were dissolved in 100 μl of DMSO; the absorbance of each well was measured at 490 nm using an automatic ELISA reader system (TECAN, CHE). The IC_{50} values were calculated using the nonlinear regression fitting models (Graph Pad, Prism Version 5). The data represented the mean of three independent experiments in triplicate and were expressed as means ± SD. The IC_{50} value was defined as the concentration at which 50% of the cells could survive.

The results were expressed as growth inhibitory concentration (IC_{50}) values and are summarized in Table 1.

4.2.2. $EGFR^{WT}$ and $EGFR^{T790M}$ kinase inhibitory assay. The most active cytotoxic compounds (**10_c, 10_d, 10_f, 11_a, 11_b, 12_b, 13_a, 13_b, 15_b, 16_a, 17_a** and **17_b**) that showed promising IC_{50} values against four cancer cell lines were further examined for their inhibitory activities against both $EGFR^{WT}$ and $EGFR^{T790M}$. Homogeneous time resolved fluorescence (HTRF) assay was applied in this test[81] with $EGFR^{WT}$ and $EGFR^{T790M}$ (Sigma). Firstly, $EGFR^{WT}$ and/or $EGFR^{T790M}$ and their substrates were incubated with the tested compounds in enzymatic buffer for 5 min. ATP (1.65 μM) was added into the reaction mixture to allow starting the enzymatic reaction. The assay was conducted for 30 min at room temperature. The reaction was stopped by the addition of detection reagents which contain EDTA. The detection step continued for 1 h, and then the IC_{50} values were determined using GraphPad Prism 5.0. Three independent experiments were performed for each concentration.

4.2.3. *In vitro* DNA-flow cytometric (cell cycle) analysis. HCT-116, HepG-2, and MCF-7 cells were exposed to the most active member **11_b** at concentrations of 3.37, 3.04, and 4.14 μM, respectively, for 24 h. Then, the tested cells were collected by trypsinization and washed in PBS. Ice-cold absolute ethanol was used for fixation of the collected cells. The cells were stained with a Cycle TESTTM PLUS DNA Reagent Kit (BD Biosciences, San Jose, CA) according to the manufacturer's instructions. Cell-cycle distribution was evaluated using a flow cytometer.[106]

4.2.4. Annexin V-FITC apoptosis assay. To detect the apoptosis induced by compound **11_b**, HCT-116, HepG-2, and MCF-7 cells were seeded and incubated overnight and then treated with compound **11_b** at concentrations of 3.37, 3.04, and 4.14 μM, respectively for 24 h. DMSO was chosen as the negative control. After that, the cells were collected and washed with PBS two successive times. The cells were exposed to centrifugation. An apoptosis detection kit (BD Biosciences, San Jose, CA) was used in this test. According to the manufacturer's protocol the cells were stained with Annexin V-FITC and propidium iodide (PI) in the binding buffer for 20min at room temperature in the dark. Using a flow cytometer, Annexin V-FITC and PI binding were analyzed. Flowjo software was used to analyze the frequencies in all quadrants.[107]

4.2.5. Caspase-3 determination. The percentage of caspase-3 activation was determined using a Caspase-Invitrogen Caspase-3 ELISA Kit (KHO1091) following the manufacturer's instructions.[108,109]

4.3. *In silico* studies

4.3.1. Docking studies. The crystal structures of the target enzymes $EGFR^{WT}$ (PDB ID: 4HJO, resolution: 2.75 Å and $EGFR^{T790M}$ (PDB ID: 3W2O, resolution: 2.35 Å) were downloaded from the Protein Data Bank (http://www.pdb.org). Molecular Operating Environment (MOE) was used for the docking analysis.[110] In these studies, the free energies and binding modes of the designed molecules against $EGFR^{WT}$ and $EGFR^{T790M}$ were determined. At first, the water molecules were removed from the crystal structures of $EGFR^{WT}$ and $EGFR^{T790M}$, retaining only one chain in each enzyme. Erlotinib and TAK-285 (the co-crystallized ligands) were utilized as references in the docking processes against both $EGFR^{WT}$ and $EGFR^{T790M}$, respectively. After that, in order to prepare the target molecules for binding with the designed compounds, the target proteins were subjected to a protonation step. Then, the hydrogen atoms were hidden to make the areas of interaction clearer. Next, the energy of all systems were minimized followed by identification of the binding pockets of the target proteins.

The structures of the designed compounds and the co-crystallized ligands, erlotinib and TAK-285, were drawn using ChemBioDraw Ultra 14.0 and saved as an SDF format. Then, the saved files were opened using MOE and 3D structures were protonated. Next, the energy of the molecules was minimized. The validation process was performed for each target by running the docking process for only the co-crystallized ligand. Low RMSD values between docked and crystal conformations indicate valid performance. The docking procedures were carried out utilizing a default protocol. In each case, 10 docked structures were generated using genetic algorithm searches. The obtained figures from the MOE were further analyzed and visualized using Discovery Studio 4.0 software.[111–113]

4.3.2. *In silico* ADMET analysis. ADMET descriptors (absorption, distribution, metabolism, excretion and toxicity) of the compounds were determined using Discovery studio 4.0. At first, the CHARMM force field was applied, then the tested compounds were prepared and the energy was minimized according to the preparation using the small molecule protocol. Then the ADMET descriptor protocol was applied to calculate the different descriptors.[112,114]

Conflicts of interest

Authors declare that no conflict of interest exist.

Acknowledgements

The authors are thankful to the Egyptian Government for financial support. A portion of this work was performed in the McKnight Brain Institute at the National High Magnetic Field Laboratory's Advanced Magnetic Resonance Imaging and Spectroscopy (AMRIS) Facility, which is supported by the US National Science Foundation Cooperative Agreement No. DMR-1644779 and the State of Florida. Some of the NMR spectra in this work were acquired using a unique 1.5 mm High Temperature Superconducting Cryogenic Probe developed with support from the US National Institutes of Health award R01EB009772. The authors would like to acknowledge the extremely valuable suggestions and technical assistance provided by Dr Mohamed R. Elnagar, Department of Pharmacology and Toxicology, Faculty of Pharmacy, Al-Azhar University, Cairo, Egypt.

References

1 M. P. Curado, L. Voti and A. M. Sortino-Rachou, Cancer registration data and quality indicators in low and middle income countries: their interpretation and potential use for the improvement of cancer care, *Cancer, Causes Control*, 2009, **20**(5), 751–756.

2 L. A. Torre, F. Bray, R. L. Siegel, J. Ferlay, J. Lortet-Tieulent and A. Jemal, Global cancer statistics, 2012, *CA-Cancer J. Clin.*, 2015, **65**(2), 87–108.

3 WHO, Cancer, Fact sheet, 2018, http://www.who.int/news-room/fact-sheets/detail/cancer (Accessed October 2018).

4 J. Taipale and P. A. Beachy, The Hedgehog and Wnt signalling pathways in cancer, *Nature*, 2001, **411**(6835), 349.

5 J. Chang, H. Ren, M. Zhao, Y. Chong, W. Zhao, Y. He, Y. Zhao, H. Zhang and C. Qi, Development of a series of novel 4-anlinoquinazoline derivatives possessing quinazoline skeleton: Design, synthesis, EGFR kinase inhibitory efficacy, and evaluation of anticancer activities in vitro, *Eur. J. Med. Chem.*, 2017, **138**, 669–688.

6 V. S. Kasture, D. S. Musmade, S. J. Aher and P. P. Patil, Tyrosine Kinases: promising targets for cancer chemotherapy, *Med. Chem. Drug Discovery*, 2012, **2**(2), 37–51.

7 M. Huang, A. Shen, J. Ding and M. Geng, Molecularly targeted cancer therapy: some lessons from the past decade, *Trends Pharmacol. Sci.*, 2014, **35**(1), 41–50.

8 M. A. Olayioye, R. M. Neve, H. A. Lane and N. E. Hynes, The ErbB signaling network: receptor heterodimerization in development and cancer, *EMBO J.*, 2000, **19**(13), 3159–3167.

9 M. L. de Castro Barbosa, L. M. Lima, R. Tesch, C. M. R. Sant'Anna, F. Totzke, M. H. Kubbutat, C. Schächtele, S. A. Laufer and E. J. Barreiro, Novel 2-chloro-4-anilino-quinazoline derivatives as EGFR and VEGFR-2 dual inhibitors, *Eur. J. Med. Chem.*, 2014, **71**, 1–14.

10 Y. Chen, J. Wu, A. Wang, Z. Qi, T. Jiang, C. Chen, F. Zou, C. Hu, W. Wang and H. Wu, Discovery of N-(5-((5-chloro-4-((2-(isopropylsulfonyl) phenyl) amino) pyrimidin-2-yl) amino)-4-methoxy-2-(4-methyl-1, 4-diazepan-1-yl) phenyl) acrylamide (CHMFL-ALK/EGFR-050) as a potent ALK/EGFR dual kinase inhibitor capable of overcoming a variety of ALK/EGFR associated drug resistant mutants in NSCLC, *Eur. J. Med. Chem.*, 2017, **139**, 674–697.

11 Y. A. Elshaier, M. A. Shaaban, M. K. A. El Hamid, M. H. Abdelrahman, M. A. Abou-Salim, S. M. Elgazwi and F. Halaweish, Design and synthesis of pyrazolo [3,4-*d*] pyrimidines: Nitric oxide releasing compounds targeting hepatocellular carcinoma, *Bioorg. Med. Chem.*, 2017, **25**(12), 2956–2970.

12 A. A. Gaber, A. H. Bayoumi, A. M. El-morsy, F. F. Sherbiny, A. B. Mehany and I. H. Eissa, Design, synthesis and anticancer evaluation of 1H-pyrazolo [3, 4-d] pyrimidine derivatives as potent EGFRWT and EGFRT790M inhibitors and apoptosis inducers, *Bioorg. Chem.*, 2018, **80**, 375–395.

13 A. M. El-Naggar, M. M. Abou-El-Regal, S. A. El-Metwally, F. F. Sherbiny and I. H. Eissa, Synthesis, characterization and molecular docking studies of thiouracil derivatives as potent thymidylate synthase inhibitors and potential anticancer agents, *Mol. Diversity*, 2017, **21**(4), 967–983.

14 I. H. Eissa, A. M. El-Naggar and M. A. El-Hashash, Design, synthesis, molecular modeling and biological evaluation of novel 1H-pyrazolo [3, 4-b] pyridine derivatives as potential anticancer agents, *Bioorg. Chem.*, 2016, **67**, 43–56.

15 H.-Q. Zhang, F.-H. Gong, J.-Q. Ye, C. Zhang, X.-H. Yue, C.-G. Li, Y.-G. Xu and L.-P. Sun, Design and discovery of 4-anilinoquinazoline-urea derivatives as dual TK inhibitors of EGFR and VEGFR-2, *Eur. J. Med. Chem.*, 2017, **125**, 245–254.

16 Z. Song, S. Huang, H. Yu, Y. Jiang, C. Wang, Q. Meng, X. Shu, H. Sun, K. Liu and Y. Li, Synthesis and biological evaluation of morpholine-substituted diphenylpyrimidine derivatives (Mor-DPPYs) as potent EGFR T790M inhibitors with improved activity toward the gefitinib-resistant non-small cell lung cancers (NSCLC), *Eur. J. Med. Chem.*, 2017, **133**, 329–339.

17 Y. Zhang, L. Chen, H. Xu, X. Li, L. Zhao, W. Wang, B. Li and X. Zhang, 6,7-Dimorpholinoalkoxy quinazoline derivatives as potent EGFR inhibitors with enhanced antiproliferative activities against tumor cells, *Eur. J. Med. Chem.*, 2018, **147**, 77–89.

18 E. A. Abdelsalam, W. A. Zaghary, K. M. Amin, N. A. Abou Taleb, A. A. Mekawey, W. M. Eldehna, H. A. Abdel-Aziz and S. F. Hammad, Synthesis and in vitro anticancer evaluation of some fused indazoles, quinazolines and quinolines as potential EGFR inhibitors, *Bioorg. Chem.*, 2019, **89**, 102985.

19 R. S. Ismail, S. M. Abou-Seri, W. M. Eldehna, N. S. Ismail, S. M. Elgazwi, H. A. Ghabbour, M. S. Ahmed, F. T. Halaweish and D. A. Abou El Ella, Novel series of 6-(2-substitutedacetamido)-4-anilinoquinazolines as EGFR-ERK signal transduction inhibitors in MCF-7 breast cancer cells, *Eur. J. Med. Chem.*, 2018, **155**, 782–796.

20 P. Bonomi, Erlotinib: a new therapeutic approach for non-small cell lung cancer, *Expert Opin. Invest. Drugs*, 2003, **12**(8), 1395–1401.
21 W. Pao, T. Y. Wang, G. J. Riely, V. A. Miller, Q. Pan, M. Ladanyi, M. F. Zakowski, R. T. Heelan, M. G. Kris and H. E. Varmus, KRAS mutations and primary resistance of lung adenocarcinomas to gefitinib or erlotinib, *PLoS Med.*, 2005, **2**(1), e17.
22 T. Celik and M. Kosker, Ocular side effects and trichomegaly of eyelashes induced by erlotinib: a case report and review of the literature, *Cont. Lens Anterior Eye*, 2015, **38**(1), 59–60.
23 M. Muhsin, J. Graham and P. Kirkpatrick, *Gefitinib*, Nature Publishing Group, 2003.
24 W. Pao, V. A. Miller, K. A. Politi, G. J. Riely, R. Somwar, M. F. Zakowski, M. G. Kris and H. Varmus, Acquired resistance of lung adenocarcinomas to gefitinib or erlotinib is associated with a second mutation in the EGFR kinase domain, *PLoS Med.*, 2005, **2**(3), 225–235.
25 S. Kobayashi, T. J. Boggon, T. Dayaram, P. A. Jänne, O. Kocher, M. Meyerson, B. E. Johnson, M. J. Eck, D. G. Tenen and B. Halmos, EGFR mutation and resistance of non–small-cell lung cancer to gefitinib, *N. Engl. J. Med.*, 2005, **352**(8), 786–792.
26 U. D. Food Administration, *FDA approves neratinib for extended adjuvant treatment of early stage HER2-positive breast cancer*, 2017, **389**(10087), 2415–2429.
27 D. Ke, L. Xiaoyun, Y. Lei, Z. Zhang, R. Xiaomei and B. S. Jeff, Targeting $EGFR^{L858R/T790M}$ and $EGFR^{L858R/T790M/C797S}$ resistance mutations in NSCLC: Current developments in medicinal chemistry, *Med. Res. Rev.*, 2018, **38**(5), 1550–1581.
28 E. L. Kwak, R. Sordella, D. W. Bell, N. Godin-Heymann, R. A. Okimoto, B. W. Brannigan, P. L. Harris, D. R. Driscoll, P. Fidias and T. J. Lynch, Irreversible inhibitors of the EGF receptor may circumvent acquired resistance to gefitinib, *Proc. Natl. Acad. Sci. U. S. A.*, 2005, **102**(21), 7665–7670.
29 J. A. Engelman, K. Zejnullahu, C.-M. Gale, E. Lifshits, A. J. Gonzales, T. Shimamura, F. Zhao, P. W. Vincent, G. N. Naumov and J. E. Bradner, PF00299804, an irreversible pan-ERBB inhibitor, is effective in lung cancer models with EGFR and ERBB2 mutations that are resistant to gefitinib, *Cancer Res.*, 2007, **67**(24), 11924–11932.
30 D. Li, L. Ambrogio, T. Shimamura, S. Kubo, M. Takahashi, L. Chirieac, R. Padera, G. Shapiro, A. Baum and F. Himmelsbach, BIBW2992, an irreversible EGFR/HER2 inhibitor highly effective in preclinical lung cancer models, *Oncogene*, 2008, **27**(34), 4702–4711.
31 L. V. Sequist, B. Besse, T. J. Lynch, V. A. Miller, K. K. Wong, B. Gitlitz, K. Eaton, C. Zacharchuk, A. Freyman and C. Powell, Neratinib, an irreversible pan-ErbB receptor tyrosine kinase inhibitor: Results of a phase II trial in patients with advanced non–small-cell lung cancer, *J. Clin. Oncol.*, 2010, **28**(18), 3076–3083.
32 Y. Kim, J. Ko, Z. Cui, A. Abolhoda, J. S. Ahn, S.-H. Ou, M.-J. Ahn and K. Park, The EGFR T790M mutation in acquired resistance to an irreversible second-generation EGFR inhibitor, *Mol. Cancer Ther.*, 2012, **11**(3), 784–791.
33 P. A. Jänne, J. C.-H. Yang, D.-W. Kim, D. Planchard, Y. Ohe, S. S. Ramalingam, M.-J. Ahn, S.-W. Kim, W.-C. Su and L. Horn, AZD9291 in EGFR inhibitor–resistant non–small-cell lung cancer, *N. Engl. J. Med.*, 2015, **372**(18), 1689–1699.
34 J. Carroll, Following lethal tox report, Boehringer scraps plans for high-speed development, kills $730M Hanmi deal, 2016, https://endpts.com/following-lethal-tox-report-boehringer-scraps-plans-for-high-speed-development-kills-730m-hanmi-deal/, (Accessed May 2019).
35 P. Callery and G. Peter, Cancer and cancer chemotherapy, in *Foye's principles of medical chemistry*, ed. A.W David and L.L Thomas, Lippincott, Williams and Wilkins, Philadelphia, 2002.
36 H. T. Abdel-Mohsen, F. A. Ragab, M. M. Ramla and H. I. El Diwani, Novel benzimidazole–pyrimidine conjugates as potent antitumor agents, *Eur. J. Med. Chem.*, 2010, **45**(6), 2336–2344.
37 H. Shao, S. Shi, D. W. Foley, F. Lam, A. Y. Abbas, X. Liu, S. Huang, X. Jiang, N. Baharin and P. M. Fischer, Synthesis, structure–activity relationship and biological evaluation of 2, 4, 5-trisubstituted pyrimidine CDK inhibitors as potential anti-tumour agents, *Eur. J. Med. Chem.*, 2013, **70**, 447–455.
38 O. Fathalla, I. Zeid, M. Haiba, A. Soliman, S. I. Abd-Elmoez and W. El-Serwy, Synthesis, antibacterial and anticancer evaluation of some pyrimidine derivatives, *World J. Chem.*, 2009, **4**(2), 127–132.
39 G. Joshi, H. Nayyar, S. Kalra, P. Sharma, A. Munshi, S. Singh and R. Kumar, Pyrimidine containing epidermal growth factor receptor kinase inhibitors: Synthesis and biological evaluation, *Chem. Biol. Drug Des.*, 2017, **90**(5), 995–1006.
40 P. Traxler, G. Bold, J. Frei, M. Lang, N. Lydon, H. Mett, E. Buchdunger, T. Meyer, M. Mueller and P. Furet, Use of a pharmacophore model for the design of EGF-R tyrosine kinase inhibitors: 4-(phenylamino) pyrazolo [3, 4-d] pyrimidines, *J. Med. Chem.*, 1997, **40**(22), 3601–3616.
41 R. Ducray, P. Ballard, B. C. Barlaam, M. D. Hickinson, J. G. Kettle, D. J. Ogilvie and C. B. Trigwell, Novel 3-alkoxy-1H-pyrazolo [3, 4-d] pyrimidines as EGFR and erbB2 receptor tyrosine kinase inhibitors, *Bioorg. Med. Chem. Lett.*, 2008, **18**(3), 959–962.
42 S. Bugge, S. J. Kaspersen, S. Larsen, U. Nonstad, G. Bjørkøy, E. Sundby and B. H. Hoff, Structure–activity study leading to identification of a highly active thienopyrimidine based EGFR inhibitor, *Eur. J. Med. Chem.*, 2014, **75**, 354–374.
43 S. N. R. Mule, S. Nurbhasha, J. Kolla, S. S. Jadav, V. Jayaprakash, L. R. Bhavanam and H. B. Bollikolla, Synthesis, biological screening and molecular docking

studies of novel 4, 6-pyrimidine derivatives as EGFR-TK inhibitors, *Med. Chem. Res.*, 2016, **25**(11), 2534–2546.

44 W. A. El-Sayed, A. E. Rashad, S. M. Awad and M. M. Ali, Synthesis and in vitro antitumor activity of new substituted thiopyrimidine acyclic nucleosides and their thioglycoside analogs, *Nucleosides, Nucleotides Nucleic Acids*, 2009, **28**(4), 261–274.

45 S. A. Morsy, A. A. Farahat, M. N. Nasr and A. S. Tantawy, Synthesis, molecular modeling and anticancer activity of new coumarin containing compounds, *Saudi Pharm. J.*, 2017, **25**(6), 873–883.

46 O. A. E.-F. M. Fathalla, M. A. Ismail, M. M. Anwar, K. A. Abouzid and A. A. Ramadan, Novel 2-thiopyrimidine derivatives as CDK2 inhibitors: molecular modeling, synthesis, and anti-tumor activity evaluation, *Med. Chem. Res.*, 2013, **22**(2), 659–673.

47 M. S. Mohamed, S. M. Awad and N. M. Ahmed, Anticancer cancer activities of 6-aryl-5-cyano-2-thiouracil derivatives, *Pharm. Res.*, 2012, **6**, 54–60.

48 G. J. Kelloff, R. A. Lubet, R. Lieberman, K. Eisenhauer, V. E. Steele, J. A. Crowell, E. T. Hawk, C. W. Boone and C. C. Sigman, Aromatase inhibitors as potential cancer chemopreventives, *Cancer Epidemiol. Biomarkers Prev.*, 1998, **7**(1), 65–78.

49 K. Wellington and S. J. Keam, Spotlight on bicalutamide 150mg in the treatment of locally advanced prostate cancer, *Drugs Aging*, 2007, **24**(2), 169–171.

50 A. M. Dos Santos, L. Cianni, D. De Vita, F. Rosini, A. Leitão, C. A. Laughton, J. Lameira and C. A. Montanari, Experimental study and computational modelling of cruzain cysteine protease inhibition by dipeptidyl nitriles, *Phys. Chem. Chem. Phys.*, 2018, **20**(37), 24317–24328.

51 L. A. Avelar, C. D. Camilo, S. de Albuquerque, W. B. Fernandes, C. Gonçalez, P. W. Kenny, A. Leitão, J. H. McKerrow, C. A. Montanari and E. V. M. Orozco, Molecular design, synthesis and trypanocidal activity of dipeptidyl nitriles as cruzain inhibitors, *PLoS Neglected Trop. Dis.*, 2015, **9**(7), 1–24.

52 Z. Zheng, P. Chen, G. Li, Y. Zhu, Z. Shi, Y. Luo, C. Zhao, Z. Fu, X. Cui and C. Ji, Mechanistic study of CBT-Cys click reaction and its application for identifying bioactive N-terminal cysteine peptides in amniotic fluid, *Chem. Sci.*, 2017, **8**(1), 214–222.

53 F. F. Fleming, L. Yao, P. Ravikumar, L. Funk and B. C. Shook, Nitrile-containing pharmaceuticals: efficacious roles of the nitrile pharmacophore, *J. Med. Chem.*, 2010, **53**(22), 7902–7917.

54 W. J. Metzler, J. Yanchunas, C. Weigelt, K. Kish, H. E. Klei, D. Xie, Y. Zhang, M. Corbett, J. K. Tamura and B. He, Involvement of DPP–IV catalytic residues in enzyme–saxagliptin complex formation, *Protein Sci.*, 2008, **17**(2), 240–250.

55 W. M. Eldehna, M. F. Abo-Ashour, A. Nocentini, P. Gratteri, I. H. Eissa, M. Fares, O. E. Ismael, H. A. Ghabbour, M. M. Elaasser and H. A. Abdel-Aziz, Novel 4/3-((4-oxo-5-(2-oxoindolin-3-ylidene) thiazolidin-2-ylidene) amino) benzenesulfonamides: Synthesis, carbonic anhydrase inhibitory activity, anticancer activity and molecular modelling studies, *Eur. J. Med. Chem.*, 2017, **139**, 250–262.

56 A. M. El-Naggar, I. H. Eissa, A. Belal and A. A. El-Sayed, Design, eco-friendly synthesis, molecular modeling and anticancer evaluation of thiazol-5 (4 H)-ones as potential tubulin polymerization inhibitors targeting the colchicine binding site, *RSC Adv.*, 2020, **10**(5), 2791–2811.

57 H. A. Mahdy, M. K. Ibrahim, A. M. Metwaly, A. Belal, A. B. Mehany, K. M. El-Gamal, A. El-Sharkawy, M. A. Elhendawy, M. M. Radwan and M. A. Elsohly, Design, synthesis, molecular modeling, in vivo studies and anticancer evaluation of quinazolin-4 (3H)-one derivatives as potential VEGFR-2 inhibitors and apoptosis inducers, *Bioorg. Chem.*, 2020, **94**, 103422.

58 A. G. A. El-Helby, H. Sakr, I. H. Eissa, A. A. Al-Karmalawy and K. El-Adl, Benzoxazole/benzothiazole–derived VEGFR–2 inhibitors: Design, synthesis, molecular docking, and anticancer evaluations, *Arch. Pharm.*, 2019, **352**(12), 1900178.

59 A. G. A. El-Helby, H. Sakr, I. H. Eissa, H. Abulkhair, A. A. Al-Karmalawy and K. El-Adl, Design, synthesis, molecular docking, and anticancer activity of benzoxazole derivatives as VEGFR–2 inhibitors, *Arch. Pharm.*, 2019, **352**(10), 1900113.

60 S. A. Elmetwally, K. F. Saied, I. H. Eissa and E. B. Elkaeed, Design, synthesis and anticancer evaluation of thieno [2, 3-d] pyrimidine derivatives as dual EGFR/HER2 inhibitors and apoptosis inducers, *Bioorg. Chem.*, 2019, **88**, 102944.

61 I. H. Eissa, A. M. El-Naggar, N. E. El-Sattar and A. S. Youssef, Design and Discovery of Novel Quinoxaline Derivatives as Dual DNA Intercalators and Topoisomerase II Inhibitors, *Anti-Cancer Agents Med. Chem. (Formerly Curr. Med. Chem. Anticancer Agents)*, 2018, **18**(2), 195–209.

62 M. Ibrahim, M. Taghour, A. Metwaly, A. Belal, A. Mehany, M. Elhendawy, M. Radwan, A. Yassin, N. El-Deeb and E. Hafez, Design, synthesis, molecular modeling and antiproliferative evaluation of novel quinoxaline derivatives as potential DNA intercalators and topoisomerase II inhibitors, *Eur. J. Med. Chem.*, 2018, **155**, 117–134.

63 I. H. Eissa, A. M. Metwaly, A. Belal, A. B. Mehany, R. R. Ayyad, K. El-Adl, H. A. Mahdy, M. S. Taghour, K. M. El-Gamal and M. E. El-Sawah, Discovery and antiproliferative evaluation of new quinoxalines as potential DNA intercalators and topoisomerase II inhibitors, *Arch. Pharm.*, 2019, **352**(11), 1900123.

64 V. Gandin, A. Ferrarese, M. Dalla Via, C. Marzano, A. Chilin and G. Marzaro, Targeting kinases with anilinopyrimidines: discovery of N-phenyl-N′-[4-(pyrimidin-4-ylamino) phenyl] urea derivatives as selective inhibitors of class III receptor tyrosine kinase subfamily, *Sci. Rep.*, 2015, **5**, 16750.

65 P. Traxler and P. Furet, Strategies toward the design of novel and selective protein tyrosine kinase inhibitors, *Pharmacol. Ther.*, 1999, **82**(2–3), 195–206.

66 J. Zhang, P. L. Yang and N. S. Gray, Targeting cancer with small molecule kinase inhibitors, *Nat. Rev. Cancer*, 2009, **9**(1), 28.
67 V. K. Sharma, P. P. Nandekar, A. Sangamwar, H. Pérez-Sánchez and S. M. Agarwal, Structure guided design and binding analysis of EGFR inhibiting analogues of erlotinib and AEE788 using ensemble docking, molecular dynamics and MM-GBSA, *RSC Adv.*, 2016, **6**(70), 65725–65735.
68 S. Mowafy, A. Galanis, Z. M. Doctor, R. M. Paranal, D. S. Lasheen, N. A. Farag, P. A. Jänne and K. A. Abouzid, Toward discovery of mutant EGFR inhibitors; Design, synthesis and in vitro biological evaluation of potent 4-arylamino-6-ureido and thioureido-quinazoline derivatives, *Bioorg. Med. Chem.*, 2016, **24**(16), 3501–3512.
69 Z. Zhao, H. Wu, L. Wang, Y. Liu, S. Knapp, Q. Liu and N. S. Gray, Exploration of type II binding mode: a privileged approach for kinase inhibitor focused drug discovery?, *ACS Chem. Biol.*, 2014, **9**(6), 1230–1241.
70 P. Furet, G. Caravatti, N. Lydon, J. P. Priestle, J. M. Sowadski, U. Trinks and P. Traxler, Modelling study of protein kinase inhibitors: binding mode of staurosporine and origin of the selectivity of CGP 52411, *J. Comput. Aided Mol. Des.*, 1995, **9**(6), 465–472.
71 Y. Liu and N. S. Gray, Rational design of inhibitors that bind to inactive kinase conformations, *Nat. Chem. Biol.*, 2006, **2**(7), 358–364.
72 P. Traxler and P. Furet, Strategies toward the design of novel and selective protein tyrosine kinase inhibitors, *Pharmacol. Ther.*, 1999, **82**(2), 195–206.
73 M. Shaquiquzzaman, S. A. Khan, M. Amir and M. M. Alam, Synthesis, anticonvulsant and neurotoxicity evaluation of some new pyrimidine-5-carbonitrile derivatives, *Saudi Pharm. J.*, 2012, **20**(2), 149–154.
74 L.-Y. Ma, L.-P. Pang, B. Wang, M. Zhang, B. Hu, D.-Q. Xue, K.-P. Shao, B.-L. Zhang, Y. Liu and E. Zhang, Design and synthesis of novel 1, 2, 3-triazole-pyrimidine hybrids as potential anticancer agents, *Eur. J. Med. Chem.*, 2014, **86**, 368–380.
75 T. Mosmann, Rapid colorimetric assay for cellular growth and survival: application to proliferation and cytotoxicity assays, *J. Immunol. Methods*, 1983, **65**(1–2), 55–63.
76 F. Denizot and R. Lang, Rapid colorimetric assay for cell growth and survival: modifications to the tetrazolium dye procedure giving improved sensitivity and reliability, *J. Immunol. Methods*, 1986, **89**(2), 271–277.
77 M. I. Thabrew, R. D. HUGHES and I. G. MCFARLANE, Screening of hepatoprotective plant components using a HepG2 cell cytotoxicity assay, *J. Pharm. Pharmacol.*, 1997, **49**(11), 1132–1135.
78 P. Li, Q. Zhang, A. Torossian, Z.-B. Li, W.-C. Xu, B. Lu and S. Fu, Simultaneous inhibition of EGFR and PI3K enhances radiosensitivity in human breast cancer, *Int. J. Radiat. Oncol., Biol., Phys.*, 2012, **83**(3), e391–e397.
79 A. Huether, M. Höpfner, V. Baradari, D. Schuppan and H. Scherübl, EGFR blockade by cetuximab alone or as combination therapy for growth control of hepatocellular cancer, *Biochem. Pharmacol.*, 2005, **70**(11), 1568–1578.
80 S. Van Schaeybroeck, J. Kyula, D. M. Kelly, A. Karaiskou-McCaul, S. A. Stokesberry, E. Van Cutsem, D. B. Longley and P. G. Johnston, Chemotherapy-induced epidermal growth factor receptor activation determines response to combined gefitinib/chemotherapy treatment in non–small cell lung cancer cells, *Mol. Cancer Ther.*, 2006, **5**(5), 1154–1165.
81 Y. Jia, C. M. Quinn, A. I. Gagnon and R. Talanian, Homogeneous time-resolved fluorescence and its applications for kinase assays in drug discovery, *Anal. Biochem.*, 2006, **356**(2), 273–281.
82 J. Wang and M. J. Lenardo, Roles of caspases in apoptosis, development, and cytokine maturation revealed by homozygous gene deficiencies, *J. Cell Sci.*, 2000, **113**(5), 753–757.
83 I. Vermes, C. Haanen, H. Steffens-Nakken and C. Reutellingsperger, A novel assay for apoptosis flow cytometric detection of phosphatidylserine expression on early apoptotic cells using fluorescein labelled annexin V, *J. Immunol. Methods*, 1995, **184**(1), 39–51.
84 W. C. Earnshaw, L. M. Martins and S. H. Kaufmann, Mammalian caspases: structure, activation, substrates, and functions during apoptosis, *Annu. Rev. Biochem.*, 1999, **68**(1), 383–424.
85 C. D. Bortner and J. A. Cidlowski, Apoptotic volume decrease and the incredible shrinking cell, *Cell Death Differ.*, 2002, **9**(12), 1307.
86 S. Zhuang, G. D. Ouedraogo and I. E. Kochevar, Downregulation of epidermal growth factor receptor signaling by singlet oxygen through activation of caspase-3 and protein phosphatases, *Oncogene*, 2003, **22**(28), 4413–4424.
87 S. S. Bae, J. H. Choi, Y. S. Oh, D. K. Perry, S. H. Ryu and P.-G. Suh, Proteolytic cleavage of epidermal growth factor receptor by caspases, *FEBS Lett.*, 2001, **491**(1–2), 16–20.
88 Y. He, J. Huang and C. Chignell, Cleavage of epidermal growth factor receptor by caspase during apoptosis is independent of its internalization, *Oncogene*, 2006, **25**(10), 1521–1531.
89 J. H. Park, Y. Liu, M. A. Lemmon and R. Radhakrishnan, Erlotinib binds both inactive and active conformations of the EGFR tyrosine kinase domain, *Biochem. J.*, 2012, **448**(3), 417–423.
90 S. Sogabe, Y. Kawakita, S. Igaki, H. Iwata, H. Miki, D. R. Cary, T. Takagi, S. Takagi, Y. Ohta and T. Ishikawa, Structure-based approach for the discovery of pyrrolo [3, 2-d] pyrimidine-based EGFR T790M/L858R mutant inhibitors, *ACS Med. Chem. Lett.*, 2012, **4**(2), 201–205.
91 H. Van De Waterbeemd and E. Gifford, ADMET in silico modelling: towards prediction paradise?, *Nat. Rev. Drug Discovery*, 2003, **2**(3), 192–204.
92 R. Mannhold, H. Kubinyi and G. Folkers, *Pharmacokinetics and metabolism in drug design*, John Wiley & Sons, 2012.
93 G. Klopman, L. R. Stefan and R. D. Saiakhov, ADME evaluation: 2. A computer model for the prediction of intestinal

absorption in humans, *Eur. J. Pharm. Sci.*, 2002, **17**(4–5), 253–263.

94 P. P. Roy and K. Roy, QSAR studies of CYP2D6 inhibitor aryloxypropanolamines using 2D and 3D descriptors, *Chem. Biol. Drug Des.*, 2009, **73**(4), 442–455.

95 T. Ghafourian and Z. Amin, QSAR models for the prediction of plasma protein binding, *BioImpacts*, 2013, **3**(1), 21.

96 V. Ramaswamy, J. W. Hooker, R. S. Withers, R. E. Nast, W. W. Brey and A. S. Edison, Development of a 13C-optimized 1.5 mm high temperature superconducting NMR probe, *J. Magn. Reson.*, 2013, **235**, 58–65.

97 S. Kambe, K. Saito, H. Kishi, A. Sakurai and H. Midorikawa, A one-step synthesis of 4-oxo-2-thioxopyrimidine derivatives by the ternary condensation of ethyl cyanoacetate, aldehydes, and thiourea, *Synthesis*, 1979, (04), 287–289.

98 S. A. Galal, A. S. Abdelsamie, H. Tokuda, N. Suzuki, A. Lida, M. M. ElHefnawi, R. A. Ramadan, M. H. Atta and H. I. El Diwani, Part I: Synthesis, cancer chemopreventive activity and molecular docking study of novel quinoxaline derivatives, *Eur. J. Med. Chem.*, 2011, **46**(1), 327–340.

99 M. S. Tolba, A. M. K. El-Dean, M. Ahmed, R. Hassanien and M. Farouk, Synthesis and antimicrobial activity of some new thienopyrimidine derivatives, *Org. Chem. (Part V)*, 2017, 229–243.

100 C. K. Jadhav, A. S. Nipate, A. V. Chate, V. D. Songire, A. P. Patil and C. H. Gill, Efficient Rapid Access to Biginelli for the Multicomponent Synthesis of 1, 2, 3, 4-Tetrahydropyrimidines in Room-Temperature Diisopropyl Ethyl Ammonium Acetate, *ACS omega*, 2019, **4**(27), 22313–22324.

101 F. M. Awadallah, G. A. Piazza, B. D. Gary, A. B. Keeton and J. C. Canzoneri, Synthesis of some dihydropyrimidine-based compounds bearing pyrazoline moiety and evaluation of their antiproliferative activity, *Eur. J. Med. Chem.*, 2013, **70**, 273–279.

102 Z. H. Khalil, A. A. A. Hafez and A. A. Ahmed, New pyrimidine derivatives: synthesis and application of thiazolo [3, 2-a]-triazolo [4, 3-a]-pyrimidine as bactericides, fungicides and bioregulators, *Phosphorus, Sulfur Silicon Relat. Elem.*, 1989, **45**(1–2), 81–93.

103 A. A. Saddik, K. M. Hassan, A. M. K. El-Dean and M. S. Abbady, Synthesis of new mercaptopyrimidines and thienopyrimidines, *Eur. Chem. Bull.*, 2015, **4**(7–9), 436–441.

104 J. Van Meerloo, G. J. Kaspers and J. Cloos, *Cell sensitivity assays: the MTT assay*, Cancer cell culture, Springer, 2011, pp. 237–245.

105 W. M. Eldehna, G. S. Hassan, S. T. Al-Rashood, T. Al-Warhi, A. E. Altyar, H. M. Alkahtani, A. A. Almehizia and H. A. Abdel-Aziz, Synthesis and in vitro anticancer activity of certain novel 1-(2-methyl-6-arylpyridin-3-yl)-3-phenylureas as apoptosis-inducing agents, *J. Enzyme Inhib. Med. Chem.*, 2019, **34**(1), 322–332.

106 S. T. Al-Rashood, A. R. Hamed, G. S. Hassan, H. M. Alkahtani, A. A. Almehizia, A. Alharbi, M. M. Al-Sanea and W. M. Eldehna, Antitumor properties of certain spirooxindoles towards hepatocellular carcinoma endowed with antioxidant activity, *J. Enzyme Inhib. Med. Chem.*, 2020, **35**(1), 831–839.

107 W. M. Eldehna, A. Nocentini, Z. M. Elsayed, T. Al-Warhi, N. Aljaeed, O. J. Alotaibi, M. M. Al-Sanea, H. A. Abdel-Aziz and C. T. Supuran, Benzofuran-based carboxylic acids as carbonic anhydrase inhibitors and antiproliferative agents against breast cancer, *ACS Med. Chem. Lett.*, 2020, **11**(5), 1022–1027.

108 Thermo Fisher Scientific, Invitrogen Caspase 3 (Cleaved) Human ELISA Kit, https://www.thermofisher.com/elisa/product/Caspase-3-Cleaved-Human-ELISA-Kit/KHO1091 (Accessed Jan. 2020).

109 Thermo Fisher Scientific, Invitrogen Caspase 9 Human ELISA Kit ELISA Kit, https://www.thermofisher.com/elisa/product/Caspase-9-Human-ELISA-Kit/BMS2025 (Accessed Jan. 2020).

110 N. Li, Y. Wang, W. Li, H. Li, L. Yang, J. Wang, H. A. Mahdy, A. Mehany, D. A. Jaiash and E. Y. Santali, Screening of Some Sulfonamide and Sulfonylurea Derivatives as Anti-Alzheimer's Agents Targeting BACE1 and PPARγ, *J. Chem.*, 2020, **2020**, 1–19.

111 M. I. Youssef, Y. Zhou, I. H. Eissa, Y. Wang, J. Zhang, L. Jiang, W. Hu, J. Qi and Z. Chen, Tetradecyl 2, 3-dihydroxybenzoate alleviates oligodendrocyte damage following chronic cerebral hypoperfusion through IGF-1 receptor, *Neurochem. Int.*, 2020, 104749.

112 M. A. El-Zahabi, E. R. Elbendary, F. H. Bamanie, M. F. Radwan, S. A. Ghareib and I. H. Eissa, Design, synthesis, molecular modeling and anti-hyperglycemic evaluation of phthalimide-sulfonylurea hybrids as PPARγ and SUR agonists, *Bioorg. Chem.*, 2019, **91**, 103115.

113 K. M. El-Gamal, A. M. El-Morsy, A. M. Saad, I. H. Eissa and M. Alswah, Synthesis, docking, QSAR, ADMET and antimicrobial evaluation of new quinoline-3-carbonitrile derivatives as potential DNA-gyrase inhibitors, *J. Mol. Struct.*, 2018, **1166**, 15–33.

114 M. K. Ibrahim, I. H. Eissa, M. S. Alesawy, A. M. Metwaly, M. M. Radwan and M. A. ElSohly, Design, synthesis, molecular modeling and anti-hyperglycemic evaluation of quinazolin-4 (3H)-one derivatives as potential PPARγ and SUR agonists, *Bioorg. Med. Chem.*, 2017, **25**(17), 4723–4744.